

# Ironing out the details of unconventional superconductivity

Rafael M. Fernandes,<sup>1</sup> Amalia I. Coldea,<sup>2</sup> Hong Ding,<sup>3,4</sup> Ian R. Fisher,<sup>5,6</sup> P. J. Hirschfeld,<sup>7</sup> and Gabriel Kotliar<sup>8,9</sup>

<sup>1</sup>*School of Physics and Astronomy, University of Minnesota, Minneapolis, MN 55455*

<sup>2</sup>*Clarendon Laboratory, Department of Physics, University of Oxford, Parks Road, Oxford OX1 3PU, UK*

<sup>3</sup>*Beijing National Laboratory for Condensed Matter Physics and Institute of Physics, Chinese Academy of Sciences, Beijing 100190, China*

<sup>4</sup>*CAS Center for Excellence in Topological Quantum Computation,  
University of Chinese Academy of Sciences, Beijing 100190, China*

<sup>5</sup>*Geballe Laboratory for Advanced Materials and Department of Applied Physics, Stanford University, Stanford, CA 94305, USA*

<sup>6</sup>*Stanford Institute for Materials and Energy Science, SLAC National Accelerator Laboratory,  
2575 Sand Hill Road, Menlo Park, California 94025, USA*

<sup>7</sup>*Department of Physics, University of Florida, 2001 Museum Rd, Gainesville, FL 32611, USA*

<sup>8</sup>*Physics and Astronomy Department, Rutgers University, Piscataway, New Jersey 08854, USA*

<sup>9</sup>*Condensed Matter Physics and Materials Science Department,  
Brookhaven National Laboratory, Upton, New York 11973, USA*

(Dated: January 7, 2022)

Superconductivity is a remarkably widespread phenomenon observed in most metals cooled down to very low temperatures. The ubiquity of such conventional superconductors, and the wide range of associated critical temperatures, is readily understood in terms of the celebrated Bardeen-Cooper-Schrieffer (BCS) theory. Occasionally, however, unconventional superconductors are found, such as the iron-based materials, which extend and defy this understanding in new and unexpected ways. In the case of the iron-based superconductors, this includes a new appreciation of the ways in which the presence of multiple atomic orbitals can manifest in unconventional superconductivity, giving rise to a rich landscape of gap structures that share the same dominant pairing mechanism. Besides superconductivity, these materials have also led to new insights into the unusual metallic state governed by the Hund’s interaction, the control and mechanisms of electronic nematicity, the impact of magnetic fluctuations and quantum criticality, and the significance of topology in correlated states. Over the thirteen years since their discovery, they have proven to be an incredibly fruitful testing ground for the development of new experimental tools and theoretical approaches, both of which have extensively influenced the wider field of quantum materials.

## I. INTRODUCTION

A comprehensive understanding of conventional superconductors, in which lattice vibrations bind electrons in Cooper pairs, is provided by the BCS-Eliashberg theory. Several families of unconventional superconductors, however, defy explanation within this paradigm, presenting a series of rich intellectual challenges. For many years, attention was split between the cuprate superconductors [1], with critical temperatures ( $T_c$ ) up to 165K, and the heavy-fermion [2] and organic superconductors [3], which typically have lower  $T_c$  values. In 2008, a new family of superconductors was discovered based on iron (Fe) [4]. The discovery was noteworthy given that Fe is generally seen as a strongly magnetic ion, and magnetism is typically considered to be antithetical to superconductivity. It rapidly became more remarkable as new members of the family were discovered with progressively higher  $T_c$  values – high enough that the materials were soon referred to as “high- $T_c$ ” (for an early review, see [5]).

A large body of evidence now indicates that these Fe-based superconductors (FeSC) are unconventional, i.e. that pairing is not driven by lattice vibrations (phonons) [6–8]. They have provided a fascinating array of new insights into the conditions of occurrence and nature of unconventional superconductivity, particularly in systems where the electrons can occupy multiple orbitals. Prior to their discovery, unconventional pairing was synonymous with Cooper pairs with non-zero angular momentum and gap nodes, exemplified, for instance, by the  $d$ -wave superconducting state realized in

cuprates [1]. In iron-based materials, however, the Cooper pairs are widely believed to have zero angular momentum, their unconventional nature arising from the different phases they take on different bands [9]. A variety of pairing structures have been observed, attributed to the same dominant pairing mechanism acting on distinct types of multi-orbital electronic structures.

Besides superconductivity, the normal state of the FeSC is also unusual. Similar to many other quantum materials, electron-electron interactions play an important role in shaping their phase diagrams. However, due to the multi-orbital character of these compounds, it is the Hund’s interaction that is believed to play the most prominent role [10]. The resulting “Hund metal” interpolates between a description of incoherent atomic states at high temperatures and coherent Fermi-surface states at low temperatures [11]. This is in contrast with the cuprates, where the onsite Hubbard repulsion dominates, or with the heavy-fermion materials, where the Kondo coupling between localized and itinerant electrons is the relevant interaction. A related concept that has emerged in studies of FeSC is that of orbital differentiation, by which distinct orbitals subjected to the same microscopic interactions experience different degrees of correlation [12–14].

It is from this correlated normal state that not only superconductivity emerges, but also other electronic ordered states. The majority of FeSC order magnetically [18]; for example,  $\text{BaFe}_2\text{As}_2$  exhibits magnetic order with a stripe pattern below a critical temperature of 134 K, although more unusual non-collinear and non-uniform spin configurations are found under

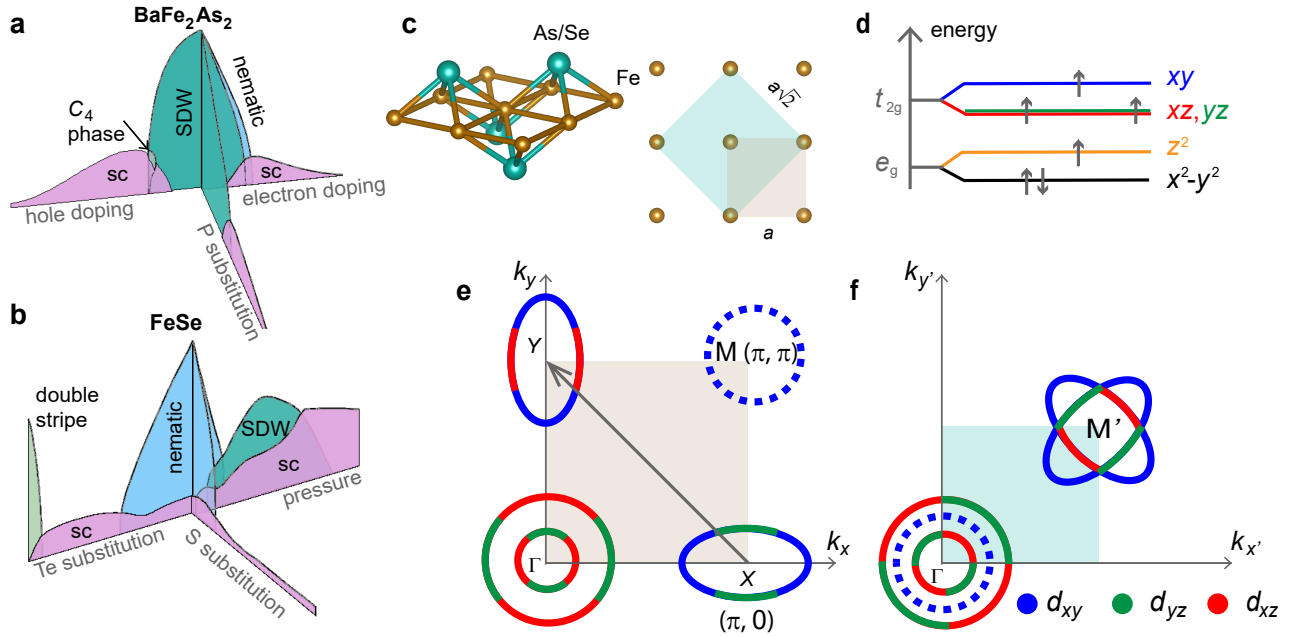


**FIG. 1. General structural and electronic properties.** Three-dimensional phase diagrams of two families of FeSC: (a)  $\text{BaFe}_2\text{As}_2$  [15] and (b)  $\text{FeSe}$  [16, 17]. The color indicates schematically the presence of different competing electronic phases – nematic, spin-density wave (SDW), double-stripe,  $C_4$  magnetic phase, and superconductivity (SC). The tuning parameter can be electron or hole doping, isoelectronic substitution (As/P or Se/S, Se/Te) or applied pressure. (c) The common structure responsible for the electronic properties of FeSC consists of Fe planes and pnictogens (As) or chalcogens (Se) outside the plane. A simplified representation considering a single Fe per unit cell is shown in gray, whereas the crystallographic unit cell containing 2 Fe per unit cell (which take into accounts the glide symmetry of the lattice) is shown in green. (d) A schematic representation of the crystal field levels of an isolated  $\text{Fe}^{2+}$  ion ( $d^6$ ) inside of a distorted  $\text{FeAs}_4$  tetrahedron [10]. The alignment of spins indicates the high spin state to fulfill Hund’s rule, but other spin states are possible. (e) The Fermi surface in the tetragonal phase (shown schematically here) consists of hole pockets at the center and of electron pockets at the corner of the (e) 1-Fe Brillouin zone and (f) 2-Fe Brillouin zone. In the latter, the two elliptical electron pockets fold along the diagonal wave-vector indicated in (e). The colors indicate the dominant orbital character of each band [6]. An additional  $d_{xy}$ -dominated hole-pocket is shown centered at  $(\pi, \pi)$  in the 1-Fe zone [(0, 0) in the 2-Fe zone] (dashed circles). The size of this pocket varies widely across materials; in some cases, such a pocket is not present. The momenta in panel (e) are in units of the inverse lattice constant  $1/a$ .

hole doping [Fig. 1(a)]. Other compounds, such as  $\text{FeSe}$ , exhibit only magnetic fluctuations at ambient pressure, but no magnetic order [Fig. 1(b)]. More ubiquitously, magnetic fluctuations at the stripe-order wave-vectors are commonly observed for superconducting compositions. The observation, by neutron scattering, of an associated resonance in the magnetic spectrum at this specific wave-vector [19, 20] has been widely interpreted as evidence both for the presence of a sign-changing superconducting gap and also for magnetic fluctuations playing a key role in the pairing interaction [21].

Another common feature found in a large number of FeSC phase diagrams is a tetragonal-to-orthorhombic structural phase transition. It often occurs either concurrently or at a higher temperature than the magnetic transition [Fig. 1(a)], although in the specific case of  $\text{FeSe}$  it occurs in the absence of magnetic order at ambient pressure [Fig. 1(b)]. A variety of experiments have revealed that lattice strain is not the primary order parameter for this phase transition, although it has the same symmetry [22]. Borrowing language from the field of liquid crystals, the state is referred to as an electronic nematic [23], in which electronic degrees of freedom drive the breaking of (discrete) rotational symmetry, while translational

symmetry is not affected. Experiments indicate that nematic fluctuations extend far across the phase diagram [24–26], motivating the question of what role, if any, nematicity plays in these materials.

The most recent surprise is the realization that several representative FeSC compounds can display topologically non-trivial band structures [27]. They have been proposed to promote various topological phenomena, such as spin-momentum-locked surface states and semi-metallic Dirac bulk states. Due to the intrinsic fully gapped unconventional superconductivity of these topological materials, they have become prime candidates in the search for robust topological superconducting states and their associated Majorana fermions.

The above brief overview brings us to an important feature of the FeSC. After 13 years of research there is a wide consensus as to the nature of the various states found in the phase diagrams. In the Landau paradigm, these phases are characterized by the symmetries that they break, and there has been little – if any – disagreement for any of the given materials as to which symmetries are broken. Yet, knowing what these states are is different from understanding how they arise and

inter-relate with each other and with the emergent superconducting state. This enables a series of well-posed questions that are, in some sense, much crisper than what can currently be asked for the other family of unconventional high- $T_c$  superconductors, the cuprates [1]. In this review, we outline what is known for sure about FeSC, and pose a series of open questions that we believe are central to understanding the origins of their unconventional superconductivity.

## II. ELECTRONIC STRUCTURE AND CORRELATIONS

All FeSC are characterized by a common structural motif comprising tetrahedrally coordinated Fe atoms arranged on a square lattice [Fig. 1(c)]. The coordinating ligands are typically from group V (the pnictogens P and As) or group VI (the chalcogens S, Se and Te). Parent compounds have a formal valence  $\text{Fe}^{2+}$ . In a description in terms of isolated atomic states, this corresponds to a  $3d^6$  electronic configuration displaying three possible spin states. Bond angles vary somewhat between compounds, differing from the perfect tetrahedral angle of  $109.5^\circ$ , thus leading to an additional splitting between the  $d_{xy}$  and  $d_{xz}/d_{yz}$  orbitals [Fig. 1(d)].

From a band theory perspective, the FeSC can be thought of as compensated semimetals, having the same number of electron-like and hole-like carriers [28]. A widely used simplified model features a Brillouin zone corresponding to the unit cell of the square Fe lattice [shaded gray area in Fig. 1(c)]. The low lying bands form the electron and hole Fermi-surface pockets displayed in Fig. 1(e) and colored according to the orbitals that contribute the largest spectral weight for that Fermi momentum [6]. More realistic models include important effects [29], such as the puckering of the As/Se atoms above and below the Fe plane, which introduces a glide plane symmetry and implies a crystallographic unit cell (and corresponding Brillouin zone) containing two Fe atoms [blue shaded areas in Figs. 1(c) and (f)] [30]. Additional effects include the spin-orbit coupling [31], which gaps out the intersections of the electron pockets in Fig. 1(f), the three-dimensional dispersion of the bands, [30], and the hybridization between the As/Se  $p$  and Fe  $d$  bands [32, 33], which is the root of several topological phenomena.

In the FeSC the charge and orbital degrees of freedom appear to be itinerant, as most compounds are metallic at all temperatures and the distinctive charge-gap and satellite features seen in oxides near a Mott transition are absent in x-ray spectroscopy [34]. At low temperatures, the normal state of the FeSC is well described by the Fermi liquid theory. The qualitative features of the quasiparticle dispersions, predicted by DFT (density functional theory) calculations and sketched in Fig. 1(e), are often similar to those detected experimentally using ARPES (angle-resolved photo-emission spectroscopy) [16, 35, 36] and quantum oscillation measurements [37]. However, the quasiparticle dispersions are generally reduced relative to the DFT calculations. Such mass enhancements, also observed in optical conductivity measurements [38], are attributed to electronic correlations, and were anticipated by DFT+DMFT (dynamical mean-field theory) calcu-

lations [39–43]. Moreover, the size of the Fermi pockets are smaller in experiments [44, 45] as compared to the DFT predictions, and in some cases this discrepancy is temperature-dependent [46, 47]. Although different mechanisms have been proposed to explain this effect [48–52], its origin remains under debate.

The correlations arise from the Coulomb repulsion between electrons, which is short-ranged due to screening. This results in an on-site Hubbard repulsion  $U$ , which penalizes the system when two electrons occupy the same site and suppresses spin fluctuations. However, because multiple orbitals are available in the FeSC, other on-site terms are also generated by the Coulomb repulsion. Among them is the Hund’s interaction  $J_H$ , which is unscreened in a solid [53] and favors the alignment of the spins of electrons in different orbitals. This leads to a correlated metallic state called a Hund metal, which is different from a Mott insulator, in that charge and orbital degrees of freedom are delocalized, while the spin degrees of freedom remain nearly localized down to low temperatures. This is illustrated schematically in Fig. 2(c), which depicts the histogram of all possible  $3d$ -Fe atomic states in a Hund metal. While the histogram extends over a wide range of electronic occupations, showcasing the itinerant nature of the charge carriers, it also displays sharp peaks at high-spin configurations, illustrating the local nature of the spins.

Fingerprints of the Hund metal phase can be seen in the FeSC upon increasing temperature ( $T$ ), where a coherence-incoherence crossover onsets [10]. In very clean materials, this manifests in the resistivity behavior, which crosses over from the characteristic Fermi-liquid  $T^2$  dependence at low temperatures to values of the order of several  $100 \mu\Omega \cdot \text{cm}$  at high temperatures [54]. In a semiclassical treatment, these values imply that the mean-free-path is of the order of the inverse of the Fermi momentum, which is not consistent with a picture of propagating Bloch waves to describe the transport properties.

The coherence-incoherence crossover can also manifest in the electronic spectrum. An example is illustrated in Fig. 2(a)-(b): at high temperatures, the  $d_{xy}$  hole-band is much fainter and flatter than the other two  $d_{xz}/d_{yz}$  hole-bands, reflecting the small coherence factor and large effective mass of the former. Upon decreasing the temperature, this  $d_{xy}$ -band, which only crosses the Fermi level in some compounds [Figs. 1(e)-(f)], becomes much sharper and thus more coherent. Such an effect, predicted theoretically [55–57], has been observed in  $\text{FeSe}_{1-x}\text{Te}_x$  and  $\text{LiFeAs}$  [36]. In extreme cases, the  $d_{xy}$  orbital could remain completely localized down to zero temperature, while the  $d_{xz}/d_{yz}$  orbitals remain coherent, giving rise to an orbital-selective Mott transition [57, 58]. The fact that the  $d_{xy}$  orbital is less coherent than the others is an example of a phenomenon called orbital differentiation [12, 17, 59], by which different orbitals are affected by correlations in distinct ways. This phenomenon is not restricted to the normal state: pronounced orbital differentiation was observed inside the superconducting phase of FeSe [14], but its origin is unsettled [17, 60, 61].

Correlations also affect the spin-excitation spectrum probed by neutron scattering, which is rather different at low and high

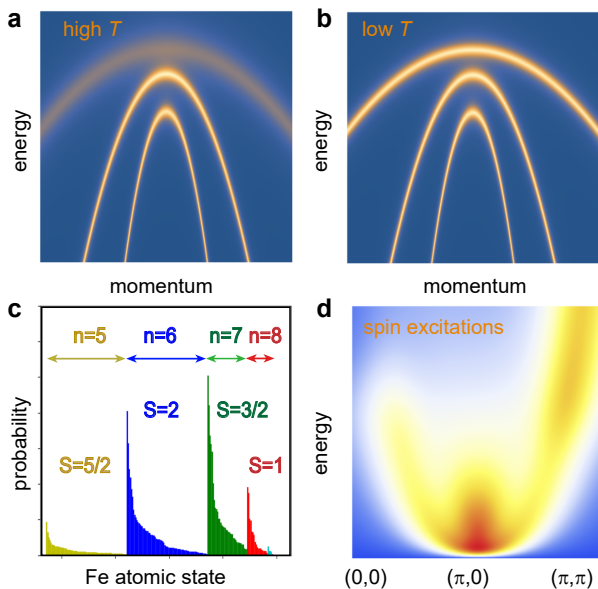


FIG. 2. **Electronic correlations and orbital differentiation.** The energy dispersions of the three hole bands along a high-symmetry direction of the 2-Fe Brillouin zone [Fig. 1(f)] at (a) high temperatures and (b) low temperatures. The topmost hole band, which has  $d_{xy}$  character, becomes incoherent at high temperatures, as represented by the faint line. At low temperatures, this band can reestablish its coherence, but its effective mass can remain sizable, as indicated by its flatness. The two other hole bands have  $d_{xz}$  and  $d_{yz}$  character. (c) Histogram of the Fe atomic states in a parent FeSC, as obtained from DMFT calculations [10]. There are  $2^{10}$  possible states involving the  $3d$  Fe orbitals. The atomic states are distributed in different colors in the histogram according to their electronic occupation  $n$ . Within a given sector  $n$  of the histogram, the states are ordered by decreasing probability; in all cases, the higher probability corresponds to the high-spin configuration for that occupation. (d) The typical momentum-resolved spin-excitation spectrum is peaked at different wave-vectors at low energies [in this case, the stripe state  $(\pi, 0)$ ] and high energies [ $(\pi, \pi)$ ].

energies [18]. In momentum space, as sketched in Fig. 2(d), at low energies the magnetic spectral weight is strongly peaked near the wave-vector of the magnetic ground state – usually, the in-plane stripe ordering vectors  $(\pi, 0)$  and  $(0, \pi)$ . As one moves towards higher energies, the magnetic spectral weight generally moves towards  $(\pi, \pi)$  [62], even though Néel order is not observed in the FeSC.

This dichotomy between low and high energies is clearly seen in the local magnetic susceptibility [18], whose imaginary part is schematically plotted in Fig. 3(a). At energies  $E_0$  of the order of 100 meV, regardless of the chemical composition, it displays a broad peak that implies a large local fluctuating magnetic moment – to be contrasted with the delocalized nature of the orbital and charge degrees of freedom. Experimental estimates give a fluctuating moment more or less uniform across different parent compounds, of about  $2\text{--}3\mu_B$  [inset of Fig. 3(a)]. In contrast, at energy scales of the order of 10 meV, the imaginary part of the local susceptibility in the paramagnetic state increases with energy [63], indicative

of Landau damping generated by the decay of spin fluctuations into particle-hole excitations – a hallmark of itinerant magnets. Indeed, the system remains metallic inside the magnetically ordered state.

Thus, while charge/orbital degrees of freedom are itinerant, the spin degrees of freedom display properties typical of strongly-correlated local-spin systems at high energies and of itinerant-spin systems at low energies. This “orbital-spin” separation [64] is the most striking feature of the Hund metal. As the temperature is lowered, this correlated metallic state displays Fermi liquid behavior and an ordered phase emerges – magnetic, nematic, or superconducting. To understand the low-energy electronic states and the resulting ordered states, it is therefore important to consider both the Fermi surface details [Fig. 1(e)], as revealed by quantum oscillation measurements [37], and the magnetic spectrum [Fig. 3(a)], as revealed by neutron scattering.

### III. MAGNETISM AT THE CROSSROADS BETWEEN ITINERANCY AND LOCALIZATION

The vast majority of FeSC parent compounds, as is the case of  $\text{BaFe}_2\text{As}_2$  in Fig. 1(a), undergo a magnetic transition to a stripe-like configuration [18]. As shown in Fig. 3(b), it consists of parallel spins along one in-plane Fe-Fe direction and antiparallel along the other. There are thus two energetically equivalent stripe states, related by an in-plane  $90^\circ$  rotation in both real-space and spin-space. The spin-orbit coupling generates magnetic anisotropies that force the spins to point parallel to the selected ordering vector [67]. As a result, a spin gap appears in the low-energy part of the local magnetic susceptibility [Fig. 3(a)], while the high-energy part is not affected. In contrast to the fluctuating moment, the ordered moment can be rather small, and it changes considerably across different compounds [inset of Fig. 3(a)] [19]. Although some parent compounds – such as  $\text{LiFeAs}$  and  $\text{FeSe}$  – do not undergo a magnetic transition, they still display low-energy fluctuations associated with the stripe magnetic state [68, 69].  $\text{FeTe}$  is one of the few parent compounds that display a different magnetic configuration – the double-stripe state of Fig. 3(c). Even in this case, upon modest substitution of Se for Te, magnetic fluctuations at the single-stripe wave-vectors emerge [70, 71].

Perturbations such as doping, isovalent chemical substitutions, and pressure not only tend to reduce the magnetic transition temperature of the pristine compositions [Fig. 1(a)], but they can also give rise to new magnetic ground states. Locally, impurities can promote puddles of Néel and other orders [72]. Globally, doping  $\text{BaFe}_2\text{As}_2$  with electrons stabilizes an incommensurate stripe order [73], whereas hole-doping promotes the so-called  $C_4$  magnetic phases [74]. The latter are linear combinations of the magnetic configurations with different stripe ordering wave-vectors that preserve the tetragonal (i.e.  $C_4$ ) symmetry of the lattice [75, 76]. They can be either the non-collinear spin-vortex crystal [Fig. 3(d)], as observed in electron-doped  $\text{CaKFe}_4\text{As}_4$  [65], or the non-uniform charge-spin density-wave [Fig. 3(e)], as observed in hole-doped  $\text{SrFe}_2\text{As}_2$  [66] (see Fig. 1(a)).

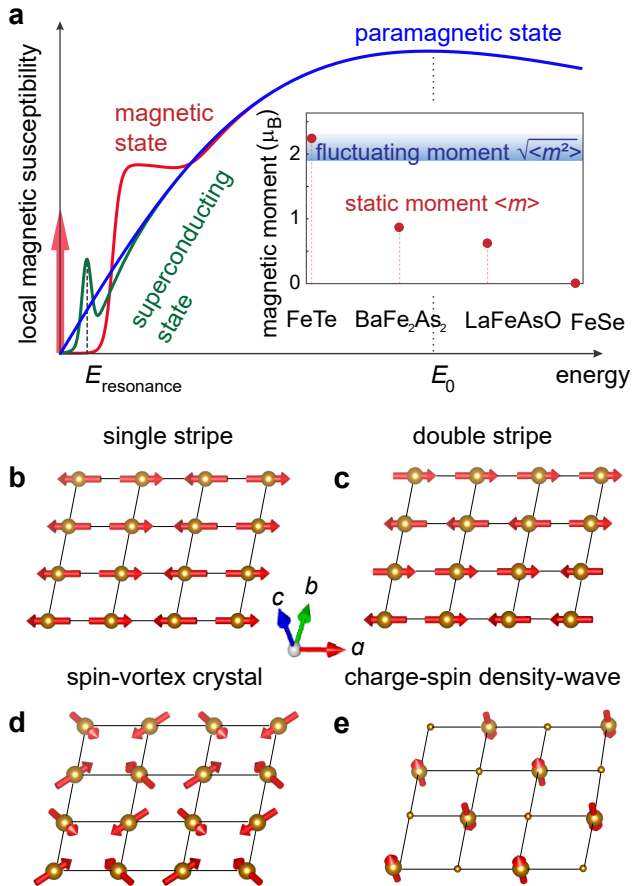


FIG. 3. **Dual local-itinerant nature of magnetism.** (a) Imaginary part of local susceptibility versus energy in a typical FeSC [18]. All FeSC show very similar high energy behavior, but differ at low energies depending on the occurrence of magnetic order (red curve and red arrow, denoting the Bragg peak) or superconductivity (green). The inset shows the variation of the static ordered moment  $\langle m \rangle$  across materials, and of the fluctuating local moment, given by the energy-integrated susceptibility  $\sqrt{\langle m^2 \rangle}$ . (b)-(c) Single-stripe and double-stripe configurations of the Fe spins. The first is realized in most FeSC, whereas the latter, in FeTe. In momentum space, they correspond respectively to Bragg peaks at  $(\pi, 0)$  [or  $(0, \pi)$ ] and  $(\pi/2, \pi/2)$  in the 1-Fe Brillouin zone. (d)-(e)  $C_4$ -symmetric spin configurations observed in electron-doped  $\text{CaKFe}_4\text{As}_4$  [65] and hole-doped  $\text{SrFe}_2\text{As}_2$  [66], respectively. They correspond to a superposition of  $(\pi, 0)$  and  $(0, \pi)$  wave-vectors resulting in either a non-collinear spin-vortex phase (d), characterized by a staggered spin-vorticity across the Fe square plaquettes, or a charge-spin density-wave phase (e), a non-uniform state with out-of-plane moments in which half of the Fe atoms display vanishing magnetization and a smaller charge density than the average (smaller yellow spheres).

Overall, the simultaneous presence of features commonly associated with localized and itinerant magnetism has motivated theoretical models adopting both a strong-coupling perspective [58, 77, 78], usually based on significant exchange interactions beyond nearest-neighbor spins, and a weak-coupling approach [49, 59, 79], often associated with

Fermi-surface nesting. Nesting refers to the situation when the hole and electron pockets in Fig. 1(e) have comparable shapes and sizes. The deterioration of the nesting conditions upon doping was invoked to explain and anticipate the onset of  $C_4$  magnetic phases and of incommensurability with doping [49, 80]. DFT has also been widely employed to investigate magnetism in FeSC. While DFT successfully captures the magnetic ground state configuration of most compounds [9, 81], it has problems in explaining the size of the ordered magnetic moment or the absence of magnetism in FeSe [82]. Advanced, beyond-DFT *ab initio* methods, have been able to address some of these problems [12, 83].

FeSC also provide a new arena to explore quantum criticality [84], a phenomenon associated with a zero-temperature second-order phase transition tuned by pressure, composition, or strain (also called a quantum critical point, QCP). Indeed, the extrapolation of the stripe magnetic transition temperature to zero near the point where the superconducting dome is peaked [Fig. 1(a)] is reminiscent of certain heavy-fermion materials [2]. Quantum criticality in those compounds is often empirically associated with non-Fermi-liquid behavior, such as a metallic resistivity whose temperature dependence deviates from the  $T^2$  Fermi-liquid behavior at low temperatures. In the FeSC, the clearest evidence for strange metal behavior associated with a putative QCP is found for  $\text{BaFe}_2(\text{As}_{1-x}\text{P}_x)_2$  [Fig. 1(a)]. There, a linear-in- $T$  resistivity and an unusual scaling of the magneto-resistance are observed above  $T_c$  near optimal doping [15, 85], and accompanied by an enhancement of the effective electron mass. Inside the superconducting dome, a sharp peak of the  $T = 0$  superconducting penetration depth is observed [15], whose origin remains unsettled [86, 87]. More generally, whether magnetic quantum criticality is a central ingredient to the phase diagram of the FeSC remains an unresolved issue, requiring further experimental and theoretical analyses.

#### IV. ELECTRONIC NEMATICITY AND VESTIGIAL ORDERS

While on symmetry grounds the nematic transition observed in most phase diagrams of FeSC is no different than a tetragonal-to-orthorhombic transition, the driving force can arise from a number of possible physical mechanisms. Quite generally, one can define order parameters that break the tetragonal symmetry of the system in different channels – spin, orbital, and lattice [Figs. 4(a)-(c)] [22]. Symmetry requires that all of these are simultaneously non-zero or zero, but cannot answer the question of which is the primary one. Indeed, direct experimental manifestations of nematic order have been reported in orbital [36], magnetic [88, 89], and elastic [25] degrees of freedom, with associated anisotropies in transport [90, 91], optical [92] and local electronic properties [93, 94]. A crucial insight came from the realization that the strain is either the primary nematic order parameter – in which case the nematic transition would be a simple structural instability – or a conjugate field to it – in which case the instability would be electronically driven. Measurements of

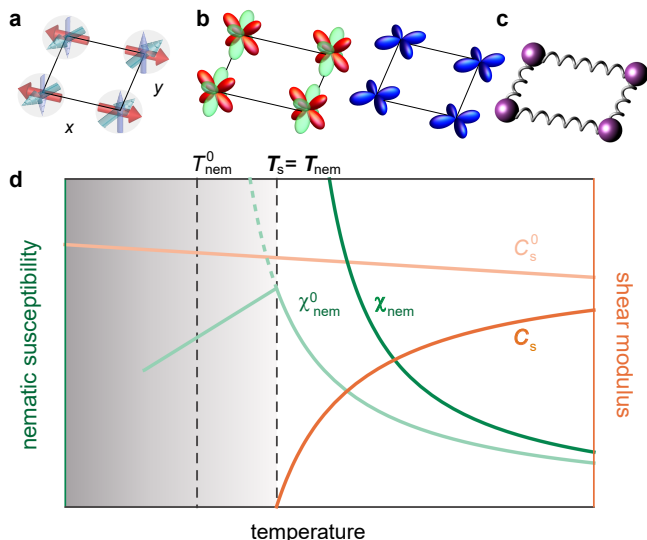


FIG. 4. **Electronic nematic order and its coupling to the lattice.** The nature of the electronic nematic transition remains a matter of investigation, and might involve one or a combination of the following mechanisms [22]. (a) In the case of spin-driven nematic order, partial melting of the stripe magnetic phase results in a state for which  $\langle \mathbf{S}_i \rangle = 0$ , where  $\mathbf{S}_i$  denotes the spin of a specific site  $i$ , but for which  $\langle \mathbf{S}_i \cdot \mathbf{S}_{i+x} \rangle = -\langle \mathbf{S}_i \cdot \mathbf{S}_{i+y} \rangle$ . (b) In the case of orbital-driven nematic order, interactions lead to a finite difference in the on-site occupancy of orbitals  $d_{xz}$  and  $d_{yz}$  (denoted by red and green on the left panel) and/or in the  $d_{xy}$  orbital hopping (blue, right panel). Symmetry ensures that all these order parameters take on a finite value in the nematic state. In all cases, an associated bare (unrenormalized) nematic susceptibility  $\chi_{\text{nem}}^0$  can be measured via a number of experimental techniques [24–26]. Coupling to the lattice results in a spontaneous strain with the same symmetry (i.e. a concomitant ferroelastic structural phase transition) at  $T_s = T_{\text{nem}}$  [panel (c)], occurring at a slightly higher temperature than the bare nematic transition temperature  $T_{\text{nem}}^0$ . It also leads to a renormalization of the nematic susceptibility  $\chi_{\text{nem}}$  for temperatures above  $T_s$ , and a softening of the elastic modulus  $C_s$  in the same symmetry channel from its bare value  $C_s^0$  [panel (d)]. Grey shading indicates the magnitude of the nematic order parameter.

the elasto-resistivity [24], as well as of the Raman spectrum [26] and elastic stiffness [25], settled this issue, establishing the dominant low-energy electronic character of the nematic state. Nevertheless, coupling to the lattice raises the critical temperature by a small amount from  $T_{\text{nem}}^0$  to  $T_{\text{nem}}$  [Fig. 4(d)].

To explain the electronic mechanism behind the nematic transition, two general scenarios have been explored, attributing it primarily to either spin or orbital degrees of freedom. This distinction, however, can become subtle, since they work in tandem [95, 96], possibly to different extents in different materials. In the simplest manifestation of the latter case, interactions spontaneously lift the degeneracy between the  $d_{xz}$  and  $d_{yz}$  orbitals [97–99], resulting in deformations of the Fermi surfaces in Fig. 1(e). In contrast, the former scenario relies on the proximity to the stripe magnetic instability, which breaks both the (discrete) rotational and translational symmetries of the lattice [22, 100, 101].

The idea is that the stripe magnetic phase melts in two stages, first restoring the broken translational symmetry and then the four-fold rotational symmetry. The intermediate paramagnetic-orthorhombic phase that onsets between the magnetic-orthorhombic and paramagnetic-tetragonal phases is the electronic nematic. Being a partially-melted magnetic phase, this has been dubbed a “vestigial” phase of the stripe magnetic state [102]. Theoretically, because it is stabilized by magnetic fluctuations, vestigial nematicity can be captured by phenomenological Ginzburg-Landau models that go beyond the mean-field approximation. Microscopically, it has been found in both localized spin [58, 100, 101, 103] and itinerant magnetic [96, 104] approaches.

The appeal of the spin-driven mechanism is that it naturally accounts for the close proximity between the stripe-magnetic and nematic phase boundaries in the phase diagrams of most FeSC. The nature of these coupled transitions – split or simultaneous, second-order or first-order – can be controlled by doping or pressure [105]. This mechanism also explains the absence of nematic order when the magnetic ground state is not the stripe one. Experimentally, the strongest evidence in favor of this scenario is the scaling between the shear modulus  $C_s$  and the NMR spin-lattice relaxation rate  $1/T_1$ , suggestive that the lattice softening is caused by magnetic fluctuations [106]. Application of this mechanism to FeSe is problematic [107], however, since stripe-magnetic order only appears when pressure is applied [108], and is completely absent in the phase diagram obtained by sulfur substitution [Fig. 1(b)]. The orbital-order scenario also faces challenges, at least in its simplest form, since ARPES measurements indicate the inadequacy of simple on-site ferro-orbital order [109, 110]. As a result, the origin of nematic order in iron chalcogenides remains an open question.

From a purely phenomenological perspective, the presence of a doping-dependent nematic phase transition implies the possibility of a nematic QCP. A variety of theoretical studies point to possible exotic non-Fermi-liquid effects proximate to such a QCP, with implications for the description of the normal state from which the superconductor emerges [111, 112]. Probing this, however, is challenging because of its proximity to a putative magnetic QCP for the vast majority of materials. The very nature of the coupled nematic-magnetic quantum phase transitions remains unsettled both experimentally and theoretically. Nevertheless, recent data unveiling power-law scaling of the nematic critical temperature as it is suppressed by doping and externally-induced strains provides strong evidence for a nematic QCP in the phase diagram of  $\text{BaFe}_2\text{As}_2$ , with an associated quantum critical regime that spans a large part of the phase diagram [113]. Another promising arena to study nematic quantum criticality is  $\text{FeSe}_{1-x}\text{S}_x$  [17, 114, 115] [Fig. 1(b)], where magnetic order is absent – although experimental evidence for possible non-Fermi liquid behavior in the vicinity of the nematic QCP remains controversial [114, 115].

Theoretically, an understanding of the nematic QCP requires incorporating two important ingredients. The first is the inevitable coupling to the lattice, which induces long-range dipolar-like nematic interactions [121]. They not only

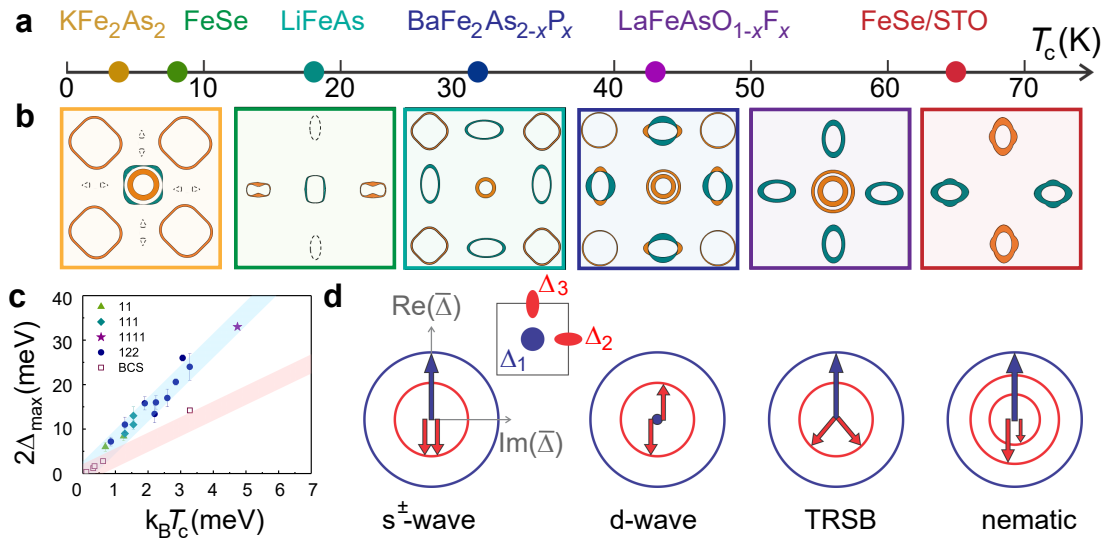


FIG. 5. **Superconducting gap structures and gap symmetries.** (a) Superconducting critical temperatures,  $T_c$ , of six canonical Fe-based superconductors. (b) Schematic gap structures for these materials in the 1-Fe Brillouin zone (borders colored according to (a)) based on weak-coupling calculations, ARPES, and STM experiments (see [6, 7, 116, 117] and references therein). The line thickness represents the magnitude of the gap, whereas the green and orange colors denote different signs. (c) Ratio between twice the maximum gap ( $2\Delta_{max}$ , based on ARPES data) and  $k_B T_c$  of FeSC, compared to that of conventional superconductors [118]. Here,  $k_B$  is the Boltzmann constant. Colored symbols correspond to some of the materials labeled in (a). The open square symbols correspond to conventional BCS superconductors. (d) Possible superconducting ground states realized in a three-band toy model with repulsive inter-band interactions [49, 119, 120]. The red (blue) arrows are associated with the complex value of the gap averaged around the electron (hole) pockets,  $\bar{\Delta}$  (see inset). TRSB denotes time-reversal symmetry breaking.

suppress critical nematic fluctuations, promoting a mean-field transition, but also change the properties of the QCP, favoring a Fermi-liquid behavior at low enough temperatures [122, 123]. The second ingredient is the ubiquitous presence of random local strains in the sample, caused by dopants and other defects [124–126]. They couple to the nematic order parameter as a random conjugate field, promoting effects typical of the random-field Ising-model. It has been argued that these effects are responsible for a deviation from Curie-Weiss behavior of the nematic susceptibility [127]. Significant progress will require models that combine long-range phonon-mediated interactions, random strain, and quantum criticality.

## V. UNCONVENTIONAL SUPERCONDUCTING STATES

The FeSC display a wide range of superconducting transition temperatures [5], as illustrated in Fig. 5(a). The largest  $T_c \approx 65$  K is observed in monolayer FeSe grown on  $SrTiO_3$ , but the precise temperature where phase-coherent superconductivity sets in is still under dispute (see [128] for a review). In contrast to cuprates, many pristine (i.e. unsubstituted) compounds display superconductivity, such as bulk FeSe, LiFeAs, and  $CaKFe_4As_4$ . In others, such as  $BaFe_2As_2$  and  $LaFeAsO$ , the competing magnetic and nematic orders need to be suppressed, e.g. via doping, chemical substitution, or pressure, to obtain superconductivity [Figs. 1(a) and (b)]. In some compounds, a second superconducting dome can be accessed by

pressure or doping [129]. In all cases, NMR measurements support a singlet pairing state [5].

Because the DFT-calculated electron-phonon coupling cannot account for the  $T_c$  of the FeSC [39, 130], an electronic mechanism has been proposed [6–8]. However, this does not preclude electron-phonon interaction, which can be enhanced by correlations [131], from playing a role in superconductivity, as it has been proposed in monolayer FeSe [132]. Quite generally, electronic repulsion forces the gap function to change sign in real/momentum space. For a large Fermi surface, such as in the cuprates, this can be accomplished by an anisotropic gap (e.g.  $d$ -wave). For multiple small Fermi pockets, such as in the FeSC, the gap can remain nearly isotropic around each Fermi surface, as long as it acquires different signs (i.e. phases) on different pockets. We refer to any gap structure that satisfies this criterion as  $s^{+-}$ -wave. In the FeSC, a strong repulsive pairing interaction is believed to be promoted by magnetic correlations associated with the nearby stripe magnetic state [Fig. 1(a)] [9]. In a weak-coupling approach, which can be implemented via RPA (random phase approximation) or (f)RG [(functional) renormalization group] calculations, the inter-pocket interaction is boosted by spin fluctuations peaked at the stripe wave-vectors  $(\pi, 0)$  and  $(0, \pi)$ , which connect the hole and electron pockets, thus overcoming the intra-pocket repulsion [6, 7, 133]. In a strong-coupling approach, pairing between next-nearest-neighbor sites is promoted by the dominant next-nearest-neighbor antiferromagnetic exchange interaction [35, 58, 77]. Although there are important differences

between the two approaches, both generally find an  $s^{+-}$  gap with opposite signs on the electron and hole pockets.

Phase-sensitive interference experiments to distinguish the  $s^{+-}$  state from the more conventional  $s^{++}$  state, which has also been proposed as mediated by orbital fluctuations [134], are challenging because the Cooper pairs have zero angular momentum in both cases. Nevertheless, there is very strong indirect evidence that an  $s^{+-}$ -wave state is realized, most notably the observation of a resonance mode in the magnetic spectrum below  $T_c$  [19, 20]. This manifests as a sharp peak in the magnetic susceptibility measured at the stripe wave-vectors and at an energy  $E_{\text{resonance}}$  below twice the gap value,  $2\Delta$  [see schematic illustration in Fig. 3(a)]. Such a feature is naturally explained if the gaps at momenta separated by the stripe wave-vectors have opposite signs [21]. Additional indirect evidence includes the observation of half-integer flux-quantum transitions in loops of polycrystalline FeSC [135] and the behavior of the momentum-integrated quasi-particle interference [117]. Moreover, the introduction of controlled disorder via irradiation has been employed to indirectly probe the gap structure. Features in agreement with an  $s^{+-}$  state have been observed, such as the lifting of accidental nodes by disorder and the rate of suppression of  $T_c$  with impurity scattering [117, 136]. The observation of in-gap bound states at nonmagnetic impurities in doped compounds is also evidence for a sign-changing gap [137].

Various gap structures can be realized under the  $s^{+-}$ -wave umbrella, depending on details of the Fermi surface and on the orbital degrees of freedom [6, 7, 133]. While the gap function generally has opposite signs on electron and hole pockets, additional sign changes between same-character pockets may occur [62]. Moreover, while ARPES observes nearly isotropic gaps in many compounds [35], accidental nodes may occur as well [116], which are well described by weak-coupling models [6, 138]. Some of these gap structures are illustrated in Fig. 5(b), in the 1-Fe Brillouin zone. They represent the leading current candidates for the gap structure of the materials in Fig. 5(a), partly motivated by theoretical considerations, but consistent with ARPES, STM, and/or neutron scattering measurements.

The variety of gap structures in Fig. 5(b) and the wide range of  $T_c$  values in Fig. 5(a) raise the question of whether there is really a common, dominant pairing mechanism in the FeSC. Evidence in favor of this comes from the dimensionless ratio  $2\Delta_{\text{max}}/(k_B T_c)$ , where  $\Delta_{\text{max}}$  is the zero-temperature value of the largest gap. As shown schematically in Fig. 5(c), this ratio usually falls between 6.0 and 8.5 for the vast majority of FeSC (blue shaded region in the figure) [118]. This is to be contrasted with the 3.5-4.5 range observed in canonical electron-phonon superconductors (red shaded region). Despite significant theoretical progress, particularly in multi-orbital weak-coupling approaches, several important questions about the superconductivity of FeSC remain open. They include establishing how the gap structure and  $T_c$  depend on specific materials parameters, such as the FeAs<sub>4</sub> tetrahedral angle [5], and explaining the seemingly universal  $2\Delta_{\text{max}}/(k_B T_c)$  ratio. Another issue is the case of compounds with only hole pockets (such as KFe<sub>2</sub>As<sub>2</sub>) or only electron pockets (such as

monolayer FeSe), which do not fall within the standard weak-coupling  $s^{+-}$  paradigm. Yet, both types of systems display superconductivity, and some of the electron-pocket-only compounds are among the highest  $T_c$ 's in all FeSC. Moreover, the relevance of magnetic fluctuations in these compounds is not well established. This begs for new approaches that can elucidate the pairing mechanism in these compounds (see e.g. [139]) and its relationship with the other FeSC.

The phase diagrams in Figs. 1(a)-(b) show that, besides stripe magnetism, nematic order is also suppressed down to zero temperature near the doping composition where  $T_c$  is the largest. This has led to an important question that remains unresolved: what role do nematic fluctuations play for the pairing state of the FeSC [22]? Theoretically, nematic fluctuations generate an attractive pairing interaction peaked at zero momentum. Hence, they can boost  $T_c$  in any symmetry channel promoted by a more dominant pairing interaction (e.g. due to spin fluctuations). Nematic fluctuations can plausibly promote superconducting order on their own, particularly near a QCP [111, 112]. However, in the clearest case of FeSe<sub>1-x</sub>S<sub>x</sub> [Fig. 1(b)], no strong change in  $T_c$  is observed at the putative nematic QCP [115], perhaps due to strong elasto-nematic coupling [122, 123].

The multi-band nature of the FeSC also opens the door for more exotic pairing states besides  $s^{+-}$ . To illustrate this, consider a toy model with one hole and two electron pockets subjected to repulsive pairing interactions. Fig. 5(d) shows schematically the possible pairing states obtained by tuning the ratio between the inter-band electron-pocket/electron-pocket and electron-pocket/hole-pocket interactions, which can be different e.g. if the orbital compositions of the Fermi pockets are distinct. When the ratio is small, an  $s^{+-}$  state is obtained: the gaps on the electron pockets are identical and have a  $\pi$  phase shift with respect to the hole-pocket gap. When the ratio is large, the ground state is  $d$ -wave: the gaps on the two electron pockets have equal magnitude but a relative  $\pi$  phase, whereas the gap on the hole pocket averages to zero. When the ratio is of order one, it is possible to realize a nematic  $s + d$  superconducting state [49], in which the electron-pockets gaps have the same phase but distinct magnitudes. This is not to be confused with the case where nematicity onsets above  $T_c$  and then coexists with superconductivity, as in FeSe. Another option is a time-reversal symmetry-breaking (TRSB)  $s + id$  superconducting state [133, 140], in which the electron-pockets gaps have equal magnitude but their relative phase is neither 0 (as in an  $s^{+-}$  state) nor  $\pi$  (as in a  $d$ -wave). A different type of TRSB pairing state, called  $s + is$  [119], has been proposed in heavily K-doped BaFe<sub>2</sub>As<sub>2</sub>, based on muon-spin rotation measurements [120].

More broadly, the variation of orbital spectral weight along the Fermi pockets [Fig. 1(e)] endows the projected pairing interaction with an angular dependence, which can favor non- $s$ -wave pairing. Microscopic calculations have in fact suggested that the  $s^{+-}$  and  $d$ -wave interactions can be comparable in strength [6, 7, 117, 133]. This is supported by the observation of certain peaks in the Raman spectrum that have been interpreted as collective  $d$ -wave excitations inside the  $s^{+-}$  state [141, 142]. Alternatively, such sharp peaks have



also been attributed to a collective nematic excitation [143]. The non-monotonic evolution of  $T_c$  with pressure in  $\text{KFe}_2\text{As}_2$  has also been interpreted as evidence for nearly-degenerate superconducting states [144]. Finally, the fact that the small Fermi energy of some FeSC is comparable to the gap value has motivated the search for strong-coupling superconductivity described not by the BCS formalism, but by the Bose-Einstein condensate (BEC) prescription of tightly-bound pre-formed Cooper pairs. Although certain properties of FeSe and  $\text{FeTe}_{1-x}\text{Se}_x$  have been described in terms of a BEC-BCS crossover [15, 145], direct evidence for pre-formed pairs remains to be seen.

## VI. TOPOLOGICAL PHENOMENA

One of the most recent developments in the field is the discovery of topological properties in some FeSC (for recent reviews, see [17, 114, 147, 148]). As schematically illustrated in Fig. 6(a), this arises from  $p$ - $d$  band inversions along the  $\Gamma$ - $Z$  direction, involving an odd-parity anionic  $p_z$ -band and an even-parity Fe  $d$ -band ( $t_{2g}$ ), as predicted by DFT [32, 33] and observed by ARPES [27, 149]. Whereas the crossings with the bands of dominant  $d_{xy}$  or  $d_{yz}$  character are protected, resulting in bulk topological Dirac semimetal states (purple shaded region), the crossing with the  $d_{xz}$ -dominated band is gapped, resulting in a topological insulating state (green shaded region). The helical surface Dirac cones emerging when the chemical potential crosses this topological gap, as well as the bulk Dirac semimetal states, were observed by ARPES in a few FeSC, most notably  $\text{FeTe}_{1-x}\text{Se}_x$  [27, 150].

Upon emergence of the  $s^{+-}$ -wave state in the bulk, superconductivity can be induced on these Dirac surface states [right panel of Fig. 6(a)]. Similarly to topological insulator/superconductor heterostructures, the surface Dirac states of the FeSC can also support Majorana zero modes (MZM) in the vortex cores of the superconducting state. The important difference is that the topological superconductivity on the FeSC surface is intrinsic and displays higher  $T_c$  values, while also avoiding the interfacial complexities of the heterostructures.

Perhaps even more significantly, the FeSC usually have small Fermi energies ( $E_F$ ) due to correlation effects, as discussed in Section II. In the particular case of  $\text{FeTe}_{1-x}\text{Se}_x$ ,  $E_F$  can be so small that it becomes comparable to the superconducting gap  $\Delta$ . This is important because, inside the vortex of any superconductor, there are discrete energy levels of  $\nu\Delta^2/E_F$ . These levels can only be distinguished in the quantum limit, where thermal broadening is smaller than the level spacing  $\Delta^2/E_F$ . Because  $\Delta$  and  $E_F$  are of similar magnitudes, the quantum limit is achievable in the FeSC [151]. In an ordinary vortex,  $\nu$  is expected to be half-integer, and the discrete levels never have zero energy [upper panels of Fig. 6(b)]. However, in a topological vortex, where Dirac surface states are incorporated,  $\nu$  is shifted to integer values due to the spin texture of the Dirac fermions [146]. As a result, a MZM emerges as the vortex bound state with zero energy [lower panels of Fig. 6(b)]. Experimentally, zero-

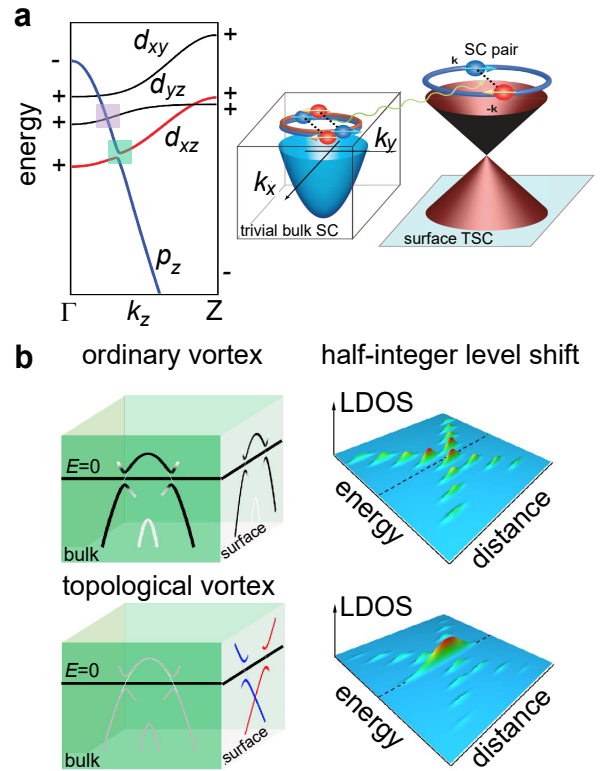


FIG. 6. **Band inversion and topological phenomena.** (a) The topological  $p$ - $d$  band inversion in the FeSC is illustrated in the left panel. The downward shift of the  $p_z$  orbital along the  $\Gamma$ - $Z$  direction causes different topological phenomena such as bulk Dirac semimetal states (purple region) and helical Dirac surface states (green region), depending on whether it crosses a  $d$  orbital of the same parity ( $d_{xy}$  or  $d_{yz}$ ) or of different parity ( $d_{xz}$ ), respectively. The right panel illustrates the topological superconductivity induced on the surface Dirac states by the bulk superconducting state. Figure reproduced from [27]. (b) In the quantum limit, which is achievable in some FeSC, discrete levels can be observed inside a vortex by probing the local density of states (LDOS) via STM. In an ordinary vortex (upper panels), these bound states are all at finite energies, whereas in a topological vortex (lower panels), a sharp zero-energy mode, called a Majorana zero mode, appears well separated from the other bound states. Figure reproduced from [146].

energy bound states as well as higher-energy discrete levels have been observed in  $\text{FeTe}_{1-x}\text{Se}_x$  via STM measurements [146, 152, 153], providing strong support for the existence of MZM.

Notwithstanding its simplicity and its intrinsic character, the FeSC Majorana platform is subjected to issues such as spatial inhomogeneity and the three-dimensional nature of the crystals. Some of these issues may be the reason why MZM are only observed in a fraction of the vortices realized inside the superconducting state [146]. Besides in the interior of vortices, signatures of Majorana fermions have also been reported in different types of lattice defects, such as interstitials [154], line vacancies [155], and crystalline domain boundaries [156]. In the latter case, a one-dimensional dispersing Majorana

rana mode was found. A potential link between the coherent-incoherent crossover and the onset of topological superconductivity in  $\text{FeTe}_{1-x}\text{Se}_x$  was also observed [157].

Several theoretical proposals for realizing other exotic topological effects based on the  $p$ - $d$  band inversion have been put forward [147], such as dispersing Majorana fermions [158] and higher-order Majorana modes in corners and hinges of samples [159]. Topological phenomena that rely only on the Fe  $3d$  orbitals have also been proposed, such as the realization of double Weyl points [160]. Theoretically, including the role of correlations in predictions of topological effects will be an important step forward, particularly in compounds as correlated as  $\text{FeTe}_{1-x}\text{Se}_x$ . The interplay with other types of electronic order, such as nematicity and magnetism, also remains little explored. Advances on the experimental front will benefit from controllable tuning of MZM and from designing a feasible pathway for braiding them [161].

## VII. OUTLOOK

After 13 years, the FeSC continue to provide a rich and unmatched framework to assess the interplay between correlations, unconventional superconductivity, magnetism, nematicity, quantum criticality, and topology. While significant advances have occurred, deep questions linger and continue to emerge as discussed in this review. New iron-based compounds continue to be regularly discovered, some with unusual structural properties promoted by the spacing layers, such as  $\text{CaKFe}_4\text{As}_4$  with centers of inversion away from the FeAs layer, the monoclinic  $\text{Ca}_{1-x}\text{La}_x\text{FeAs}_2$  [162], and the insulating ladder compound  $\text{BaFe}_2\text{Se}_3$  [163, 164]. Pnictide compounds based not on iron, but on nickel, cobalt, and manganese have also been systematically grown and studied. These systems offer new opportunities to address some of those unanswered questions and, at the same time, venture into unexplored directions.

Many of the theoretical and experimental advances spurred by studies of the FeSC have found fertile ground in other quantum materials. The discovery of this completely new class of compounds provided a fresh testbed to compare state-of-the-art methods in correlated electronic structure calculations against a large number of experimental results. The concept of a Hund metal has also been used to explain the normal-state properties of a broad range of quantum materials, such as  $\text{Sr}_2\text{RuO}_4$  [11]. Multi-orbital pairing models, such as RPA, FLEX, and (f)RG, have been extensively employed to shed new light on multi-band superconductors, such as ruthenates and nickelates. The concept of vestigial orders and the associated phenomenological models have led to important new insights into antiferromagnetic and topological superconducting materials [102]. Experimentally, symmetry-breaking strain has been recognized as a uniquely appropriate tool to probe electronic nematic order. Strain-based techniques applied to transport, thermodynamic, scattering, spectroscopic and local probe measurements are now considered mainstream, and have enabled the identification and manipu-

lation of electronic nematicity and a variety of other electronic states in disparate materials such as cuprates and  $f$ -electron systems – which have emerged as promising candidates to realize nematic quantum criticality [165].

Conceptually, FeSC emphasize a type of correlated state – the Hund metal – that is different from a Mott insulator or a heavy-fermion metal. Although at low temperatures and energies it behaves as a Fermi liquid, it displays a wide temperature range where charge/orbital degrees of freedom seem itinerant but spins seem localized. On the one hand, approaches that go beyond DFT and consider the frequency dependence of the electronic interactions (such as DMFT) have been successful in describing effects related to the intermediate-energy range, such as the large fluctuating local moment and the coherent-incoherent crossover experience by the  $d_{xy}$  orbital. On the other hand, phenomenological models that go beyond mean-field and perturbative approaches such as (f)RG and RPA, which focus on the long-wavelength momentum dependence of the electronic interactions, have nicely captured low-energy phenomena that emerge when the system enters its Fermi-liquid regime, such as the structure of the magnetic, superconducting, and nematic order parameters. Significant progress in this field – and in other similar types of quantum materials – will require novel ideas that can seamlessly combine long-wavelength theories with more accurate correlated electronic structure methods, thus smoothly interpolating between the intermediate- and low-energy behaviors.

## ACKNOWLEDGMENTS

We thank all our co-authors and collaborators with whom we had many fruitful discussions since the discovery of the iron-based superconductors. We particularly thank H. Miao and T. H. Lee (Figure 2), M. Christensen (Figure 4) and L.-Y. Kong (Figure 6) for their assistance in making some of the figures. R.M.F. was supported by the U.S. Department of Energy, Office of Science, Basic Energy Sciences, Materials Science and Engineering Division, under Award No. DE-SC0020045. A.I.C. acknowledges an EPSRC Career Acceleration Fellowship (EP/I004475/1) and the Oxford Centre for Applied Superconductivity (CFAS) for financial support. A.I.C. is grateful to the KITP program *correlated20*, which was supported in part by the National Science Foundation under Grant No. NSF PHY-1748958. H.D. is supported by the National Natural Science Foundation of China (Grant Nos. 11888101, 11674371), the Strategic Priority Research Program of Chinese Academy of Sciences, China (Grant Nos. XDB28000000, XDB07000000), and the Beijing Municipal Science & Technology Commission, China (Grant No. Z191100007219012). I.R.F. was supported by the Department of Energy, Office of Basic Energy Sciences, under contract DE-AC02-76SF00515. P.J.H. was supported by the U.S. Department of Energy, Office of Basic Sciences under Grant No. DE-FG02-05ER46236. G.K. was supported by NSF DMR-1733071.

- [1] B. Keimer, S. A. Kivelson, M. R. Norman, S. Uchida, and J. Zaanen, From quantum matter to high-temperature superconductivity in copper oxides, *Nature* **518**, 179 (2015).
- [2] B. White, J. Thompson, and M. Maple, Unconventional superconductivity in heavy-fermion compounds, *Physica C: Superconductivity and its Applications* **514**, 246 (2015).
- [3] J. Singleton and C. Mielke, Quasi-two-dimensional organic superconductors: A review, *Contemporary Physics* **43**, 63 (2002).
- [4] Y. Kamihara, T. Watanabe, M. Hirano, and H. Hosono, Iron-Based Layered Superconductor  $\text{LaO}_{1-x}\text{F}_x\text{FeAs}$  ( $x = 0.05 - 0.12$ ) with  $T_c = 26$  K, *Journal of the American Chemical Society* **130**, 3296 (2008).
- [5] D. C. Johnston, The puzzle of high temperature superconductivity in layered iron pnictides and chalcogenides, *Advances in Physics* **59**, 803 (2010).
- [6] P. J. Hirschfeld, M. M. Korshunov, and I. I. Mazin, Gap symmetry and structure of Fe-based superconductors, *Reports on Progress in Physics* **74**, 124508 (2011).
- [7] A. V. Chubukov, Pairing Mechanism in Fe-Based Superconductors, *Annual Review of Condensed Matter Physics* **3**, 57 (2012).
- [8] F. Wang and D.-H. Lee, The Electron-Pairing Mechanism of Iron-Based Superconductors, *Science* **332**, 200 (2011).
- [9] I. I. Mazin, D. J. Singh, M. D. Johannes, and M. H. Du, Unconventional Superconductivity with a Sign Reversal in the Order Parameter of  $\text{LaFeAsO}_{1-x}\text{F}_x$ , *Phys. Rev. Lett.* **101**, 057003 (2008).
- [10] K. Haule and G. Kotliar, Coherence–incoherence crossover in the normal state of iron oxypnictides and importance of Hund's rule coupling, *New Journal of Physics* **11**, 025021 (2009).
- [11] A. Georges, L. d. Medici, and J. Mravlje, Strong Correlations from Hund's Coupling, *Annual Review of Condensed Matter Physics* **4**, 137 (2013).
- [12] Z. Yin, K. Haule, and G. Kotliar, Kinetic frustration and the nature of the magnetic and paramagnetic states in iron pnictides and iron chalcogenides, *Nature materials* **10**, 932 (2011).
- [13] L. de' Medici, Weak and strong correlations in Fe superconductors, in *Iron-Based Superconductivity*, edited by P. D. Johnson, G. Xu, and W.-G. Yin (Springer International Publishing, Cham, 2015) pp. 409–441.
- [14] P. O. Sprau, A. Kostin, A. Kreisel, A. E. Böhrer, V. Taufour, P. C. Canfield, S. Mukherjee, P. J. Hirschfeld, B. M. Andersen, and J. C. S. Davis, Discovery of orbital-selective Cooper pairing in FeSe, *Science* **357**, 75 (2017).
- [15] T. Shibauchi, A. Carrington, and Y. Matsuda, A quantum critical point lying beneath the superconducting dome in iron pnictides, *Annual Review of Condensed Matter Physics* **5**, 113 (2014).
- [16] A. I. Coldea and M. D. Watson, The Key Ingredients of the Electronic Structure of FeSe, *Annual Review of Condensed Matter Physics* **9**, 125 (2018).
- [17] A. Kreisel, P. J. Hirschfeld, and B. M. Andersen, On the Remarkable Superconductivity of FeSe and Its Close Cousins, *Symmetry* **12**, 10.3390/sym12091402 (2020).
- [18] P. Dai, Antiferromagnetic order and spin dynamics in iron-based superconductors, *Rev. Mod. Phys.* **87**, 855 (2015).
- [19] M. D. Lumsden and A. D. Christianson, Magnetism in Fe-based superconductors, *Journal of Physics: Condensed Matter* **22**, 203203 (2010).
- [20] D. S. Inosov, Spin fluctuations in iron pnictides and chalcogenides: From antiferromagnetism to superconductivity, *Comptes Rendus Physique* **17**, 60 (2016).
- [21] D. J. Scalapino, A common thread: The pairing interaction for unconventional superconductors, *Rev. Mod. Phys.* **84**, 1383 (2012).
- [22] R. M. Fernandes, A. V. Chubukov, and J. Schmalian, What drives nematic order in iron-based superconductors?, *Nature Physics* **10**, 97 (2014).
- [23] E. Fradkin, S. A. Kivelson, M. J. Lawler, J. P. Eisenstein, and A. P. Mackenzie, Nematic Fermi Fluids in Condensed Matter Physics, *Annual Review of Condensed Matter Physics* **1**, 153 (2010).
- [24] J.-H. Chu, H.-H. Kuo, J. G. Analytis, and I. R. Fisher, Divergent nematic susceptibility in an iron arsenide superconductor, *Science* **337**, 710 (2012).
- [25] A. E. Bohmer and C. Meingast, Electronic nematic susceptibility of iron-based superconductors, *Comptes Rendus Physique* **17**, 90 (2016).
- [26] Y. Gallais and I. Paul, Charge nematicity and electronic raman scattering in iron-based superconductors, *Comptes Rendus Physique* **17**, 113 (2016).
- [27] P. Zhang, K. Yaji, T. Hashimoto, Y. Ota, T. Kondo, K. Okazaki, Z. Wang, J. Wen, G. D. Gu, H. Ding, and S. Shin, Observation of topological superconductivity on the surface of an iron-based superconductor, *Science* **360**, 182 (2018).
- [28] D. J. Singh and M.-H. Du, Density Functional Study of  $\text{LaFeAsO}_{1-x}\text{F}_x$ : A Low Carrier Density Superconductor Near Itinerant Magnetism, *Phys. Rev. Lett.* **100**, 237003 (2008).
- [29] V. Cvetkovic and O. Vafek, Space group symmetry, spin-orbit coupling, and the low-energy effective Hamiltonian for iron-based superconductors, *Phys. Rev. B* **88**, 134510 (2013).
- [30] H. Eschrig and K. Koepf, Tight-binding models for the iron-based superconductors, *Phys. Rev. B* **80**, 104503 (2009).
- [31] S. Borisenko, D. Evtushinsky, Z.-H. Liu, I. Morozov, R. Kappenberger, S. Wurmehl, B. Büchner, A. Yaresko, T. Kim, M. Hoesch, *et al.*, Direct observation of spin-orbit coupling in iron-based superconductors, *Nature Physics* **12**, 311 (2016).
- [32] Z. Wang, P. Zhang, G. Xu, L. K. Zeng, H. Miao, X. Xu, T. Qian, H. Weng, P. Richard, A. V. Fedorov, H. Ding, X. Dai, and Z. Fang, Topological nature of the  $\text{FeSe}_{0.5}\text{Te}_{0.5}$  superconductor, *Phys. Rev. B* **92**, 115119 (2015).
- [33] G. Xu, B. Lian, P. Tang, X.-L. Qi, and S.-C. Zhang, Topological Superconductivity on the Surface of Fe-Based Superconductors, *Phys. Rev. Lett.* **117**, 047001 (2016).
- [34] W. L. Yang, A. P. Sorini, C.-C. Chen, B. Moritz, W.-S. Lee, F. Vernay, P. Olalde-Velasco, J. D. Denlinger, B. Delley, J.-H. Chu, J. G. Analytis, I. R. Fisher, Z. A. Ren, J. Yang, W. Lu, Z. X. Zhao, J. van den Brink, Z. Hussain, Z.-X. Shen, and T. P. Devereaux, Evidence for weak electronic correlations in iron pnictides, *Phys. Rev. B* **80**, 014508 (2009).
- [35] P. Richard, T. Qian, and H. Ding, ARPES measurements of the superconducting gap of Fe-based superconductors and their implications to the pairing mechanism, *Journal of Physics: Condensed Matter* **27**, 293203 (2015).
- [36] M. Yi, Y. Zhang, Z.-X. Shen, and D. Lu, Role of the orbital degree of freedom in iron-based superconductors, *npj Quantum Materials* **2**, 57 (2017).
- [37] A. Carrington, Quantum oscillation studies of the Fermi surface of iron-pnictide superconductors, *Reports on Progress in Physics* **74**, 124507 (2011).

- [38] M. Qazilbash, J. Hamlin, R. Baumbach, L. Zhang, D. J. Singh, M. Maple, and D. Basov, Electronic correlations in the iron pnictides, *Nature Physics* **5**, 647 (2009).
- [39] K. Haule, J. H. Shim, and G. Kotliar, Correlated Electronic Structure of  $\text{LaO}_{1-x}\text{F}_x\text{FeAs}$ , *Phys. Rev. Lett.* **100**, 226402 (2008).
- [40] S. L. Skornyakov, A. V. Efremov, N. A. Skorikov, M. A. Korotin, Y. A. Izyumov, V. I. Anisimov, A. V. Kozhevnikov, and D. Vollhardt, Classification of the electronic correlation strength in the iron pnictides: The case of the parent compound  $\text{BaFe}_2\text{As}_2$ , *Phys. Rev. B* **80**, 092501 (2009).
- [41] P. Werner, M. Casula, T. Miyake, F. Aryasetiawan, A. J. Millis, and S. Biermann, Satellites and large doping and temperature dependence of electronic properties in hole-doped  $\text{BaFe}_2\text{As}_2$ , *Nature Physics* **8**, 331 (2012).
- [42] J. Ferber, K. Foyevtsova, R. Valentí, and H. O. Jeschke, LDA + DMFT study of the effects of correlation in  $\text{LiFeAs}$ , *Phys. Rev. B* **85**, 094505 (2012).
- [43] A. van Roekeghem, P. Richard, H. Ding, and S. Biermann, Spectral properties of transition metal pnictides and chalcogenides: Angle-resolved photoemission spectroscopy and dynamical mean-field theory, *Comptes Rendus Physique* **17**, 140 (2016).
- [44] A. I. Coldea, J. D. Fletcher, A. Carrington, J. G. Analytis, A. F. Bangura, J.-H. Chu, A. S. Erickson, I. R. Fisher, N. E. Hussey, and R. D. McDonald, Fermi Surface of Superconducting  $\text{LaFePO}$  Determined from Quantum Oscillations, *Phys. Rev. Lett.* **101**, 216402 (2008).
- [45] A. Kordyuk, V. Zabolotnyy, D. Evtushinsky, A. Yaresko, B. Büchner, and S. Borisenko, Electronic band structure of ferro-pnictide superconductors from ARPES experiment, *Journal of Superconductivity and Novel Magnetism* **26**, 2837 (2013).
- [46] R. S. Dhaka, S. E. Hahn, E. Razzoli, R. Jiang, M. Shi, B. N. Harmon, A. Thaler, S. L. Bud'ko, P. C. Canfield, and A. Kaminski, Unusual Temperature Dependence of Band Dispersion in  $\text{Ba}(\text{Fe}_{1-x}\text{Ru}_x)_2\text{As}_2$  and its Consequences for Antiferromagnetic Ordering, *Phys. Rev. Lett.* **110**, 067002 (2013).
- [47] V. Brouet, P.-H. Lin, Y. Texier, J. Bobroff, A. Taleb-Ibrahimi, P. Le Fèvre, F. Bertran, M. Casula, P. Werner, S. Biermann, F. Rullier-Albenque, A. Forget, and D. Colson, Large Temperature Dependence of the Number of Carriers in Co-Doped  $\text{BaFe}_2\text{As}_2$ , *Phys. Rev. Lett.* **110**, 167002 (2013).
- [48] L. Ortenzi, E. Cappelluti, L. Benfatto, and L. Pietronero, Fermi-Surface Shrinking and Interband Coupling in Iron-Based Pnictides, *Phys. Rev. Lett.* **103**, 046404 (2009).
- [49] R. M. Fernandes and A. V. Chubukov, Low-energy microscopic models for iron-based superconductors: a review, *Reports on Progress in Physics* **80**, 014503 (2016).
- [50] K. Zantout, S. Backes, and R. Valentí, Effect of Nonlocal Correlations on the Electronic Structure of  $\text{LiFeAs}$ , *Phys. Rev. Lett.* **123**, 256401 (2019).
- [51] S. Bhattacharyya, K. Björnson, K. Zantout, D. Steffensen, L. Fanfarillo, A. Kreisel, R. Valentí, B. M. Andersen, and P. J. Hirschfeld, Nonlocal correlations in iron pnictides and chalcogenides, *Phys. Rev. B* **102**, 035109 (2020).
- [52] M. Kim, H. Miao, S. Choi, M. Zingl, A. Georges, and G. Kotliar, On the Spatial Locality of Electronic Correlations in  $\text{LiFeAs}$ , arXiv:2009.10577 (2020).
- [53] D. van der Marel and G. A. Sawatzky, Electron-electron interaction and localization in d and f transition metals, *Phys. Rev. B* **37**, 10674 (1988).
- [54] F. Hardy, A. E. Böhmer, D. Aoki, P. Burger, T. Wolf, P. Schweiss, R. Heid, P. Adelmann, Y. X. Yao, G. Kotliar, J. Schmalian, and C. Meingast, Evidence of Strong Correlations and Coherence-Incoherence Crossover in the Iron Pnictide Superconductor  $\text{KFe}_2\text{As}_2$ , *Phys. Rev. Lett.* **111**, 027002 (2013).
- [55] Z. P. Yin, K. Haule, and G. Kotliar, Fractional power-law behavior and its origin in iron-chalcogenide and ruthenate superconductors: Insights from first-principles calculations, *Phys. Rev. B* **86**, 195141 (2012).
- [56] R. Yu and Q. Si, Orbital-Selective Mott Phase in Multiorbital Models for Alkaline Iron Selenides  $\text{K}_{1-x}\text{Fe}_{2-y}\text{Se}_2$ , *Phys. Rev. Lett.* **110**, 146402 (2013).
- [57] L. de' Medici, G. Giovannetti, and M. Capone, Selective Mott Physics as a Key to Iron Superconductors, *Phys. Rev. Lett.* **112**, 177001 (2014).
- [58] Q. Si, R. Yu, and E. Abrahams, High-temperature superconductivity in iron pnictides and chalcogenides, *Nature Reviews Materials* **1**, 16017 (2016).
- [59] E. Bascones, B. Valenzuela, and M. J. Calderón, Magnetic interactions in iron superconductors: A review, *Comptes Rendus Physique* **17**, 36 (2016).
- [60] L. C. Rhodes, M. D. Watson, A. A. Haghighirad, D. V. Evtushinsky, M. Eschrig, and T. K. Kim, Scaling of the superconducting gap with orbital character in  $\text{FeSe}$ , *Phys. Rev. B* **98**, 180503 (2018).
- [61] D. Liu, C. Li, J. Huang, B. Lei, L. Wang, X. Wu, B. Shen, Q. Gao, Y. Zhang, X. Liu, Y. Hu, Y. Xu, A. Liang, J. Liu, P. Ai, L. Zhao, S. He, L. Yu, G. Liu, Y. Mao, X. Dong, X. Jia, F. Zhang, S. Zhang, F. Yang, Z. Wang, Q. Peng, Y. Shi, J. Hu, T. Xiang, X. Chen, Z. Xu, C. Chen, and X. J. Zhou, Orbital Origin of Extremely Anisotropic Superconducting Gap in Nematic Phase of  $\text{FeSe}$  Superconductor, *Phys. Rev. X* **8**, 031033 (2018).
- [62] Z. Yin, K. Haule, and G. Kotliar, Spin dynamics and orbital-antiphase pairing symmetry in iron-based superconductors, *Nature Physics* **10**, 845 (2014).
- [63] M. Wang, C. Zhang, X. Lu, G. Tan, H. Luo, Y. Song, M. Wang, X. Zhang, E. Goremychkin, T. Perring, T. Maier, Z. Yin, K. Haule, G. Kotliar, and P. Dai, Doping dependence of spin excitations and its correlations with high-temperature superconductivity in iron pnictides, *Nature Communications* **4**, 2874 (2013).
- [64] K. M. Stadler, Z. P. Yin, J. von Delft, G. Kotliar, and A. Weichselbaum, Dynamical mean-field theory plus numerical renormalization-group study of spin-orbital separation in a three-band hund metal, *Phys. Rev. Lett.* **115**, 136401 (2015).
- [65] W. R. Meier, Q.-P. Ding, A. Kreyssig, S. L. Bud'ko, A. Sapkota, K. Kothapalli, V. Borisov, R. Valentí, C. D. Batista, P. P. Orth, R. M. Fernandes, A. I. Goldman, Y. Furukawa, A. E. Böhmer, and P. C. Canfield, Hedgehog spin-vortex crystal stabilized in a hole-doped iron-based superconductor, *npj Quantum Materials* **3**, 5 (2018).
- [66] J. M. Allred, K. M. Taddei, D. E. Bugaris, M. J. Krogstad, S. H. Lapidus, D. Y. Chung, H. Claus, M. G. Kanatzidis, D. E. Brown, J. Kang, R. M. Fernandes, I. Eremin, S. Rosenkranz, O. Chmaissem, and R. Osborn, Double-Q spin-density wave in iron arsenide superconductors, *Nature Physics* **12**, 493 (2016).
- [67] M. H. Christensen, J. Kang, B. M. Andersen, I. Eremin, and R. M. Fernandes, Spin reorientation driven by the interplay between spin-orbit coupling and Hund's rule coupling in iron pnictides, *Phys. Rev. B* **92**, 214509 (2015).
- [68] N. Qureshi, P. Steffens, Y. Drees, A. C. Komarek, D. Lamago, Y. Sidis, L. Harnagea, H.-J. Grafe, S. Wurmehl, B. Büchner, and M. Braden, Inelastic Neutron-Scattering Measurements

- of Incommensurate Magnetic Excitations on Superconducting LiFeAs Single Crystals, *Phys. Rev. Lett.* **108**, 117001 (2012).
- [69] Q. Wang, Y. Shen, B. Pan, X. Zhang, K. Ikeuchi, K. Iida, A. Christianson, H. Walker, D. Adroja, M. Abdel-Hafiez, X. Chen, D. Chareev, A. Vasiliev, and J. Zhao, Magnetic ground state of FeSe, *Nature Communications* **7**, 12182 (2016).
- [70] M. D. Lumsden, A. D. Christianson, E. Goremychkin, S. E. Nagler, H. Mook, M. B. Stone, D. L. Abernathy, T. Guidi, G. J. MacDougall, C. de la Cruz, A. Sefat, M. McGuire, B. Sales, and D. Mandrus, Evolution of spin excitations into the superconducting state in  $\text{FeTe}_{1-x}\text{Se}_x$ , *Nature Physics* **6**, 182 (2010).
- [71] T. Liu, J. Hu, B. Qian, D. Fobes, Z. Q. Mao, W. Bao, M. Reehuis, S. Kimber, K. Prokeš, S. Matas, D. Argyriou, A. Hiess, A. Rotaru, H. Pham, L. Spinu, Y. Qiu, V. Thampy, A. Savici, J. Rodriguez, and C. Broholm, From  $(\pi, \pi)$  magnetic order to superconductivity with  $(\pi, \pi)$  magnetic resonance in  $\text{Fe}_{1.02}\text{Te}_{1-x}\text{Se}_x$ , *Nature Materials* **9**, 718 (2010).
- [72] M. N. Gastiasoro and B. M. Andersen, Enhancement of magnetic stripe order in iron-pnictide superconductors from the interaction between conduction electrons and magnetic impurities, *Phys. Rev. Lett.* **113**, 067002 (2014).
- [73] D. K. Pratt, M. G. Kim, A. Kreyssig, Y. B. Lee, G. S. Tucker, A. Thaler, W. Tian, J. L. Zarestky, S. L. Bud'ko, P. C. Canfield, B. N. Harmon, A. I. Goldman, and R. J. McQueeney, Incommensurate Spin-Density Wave Order in Electron-Doped  $\text{BaFe}_2\text{As}_2$  Superconductors, *Phys. Rev. Lett.* **106**, 257001 (2011).
- [74] E. Sheveleva, B. Xu, P. Marsik, F. Lyzwa, B. P. P. Mallett, K. Willa, C. Meingast, T. Wolf, T. Shevtsova, Y. G. Pashkevich, and C. Bernhard, Muon spin rotation and infrared spectroscopy study of  $\text{Ba}_{1-x}\text{Na}_x\text{Fe}_2\text{As}_2$ , *Phys. Rev. B* **101**, 224515 (2020).
- [75] J. Lorenzana, G. Seibold, C. Ortix, and M. Grilli, Competing Orders in FeAs Layers, *Phys. Rev. Lett.* **101**, 186402 (2008).
- [76] R. M. Fernandes, S. A. Kivelson, and E. Berg, Vestigial chiral and charge orders from bidirectional spin-density waves: Application to the iron-based superconductors, *Phys. Rev. B* **93**, 014511 (2016).
- [77] K. Seo, B. A. Bernevig, and J. Hu, Pairing symmetry in a two-orbital exchange coupling model of oxypnictides, *Phys. Rev. Lett.* **101**, 206404 (2008).
- [78] P. Dai, J. Hu, and E. Dagotto, Magnetism and its microscopic origin in iron-based high-temperature superconductors, *Nature Physics* **8**, 709 (2012).
- [79] I. Eremin and A. V. Chubukov, Magnetic degeneracy and hidden metallicity of the spin-density-wave state in ferropnictides, *Phys. Rev. B* **81**, 024511 (2010).
- [80] A. B. Vorontsov, M. G. Vavilov, and A. V. Chubukov, Superconductivity and spin-density waves in multiband metals, *Phys. Rev. B* **81**, 174538 (2010).
- [81] T. Yildirim, Origin of the 150-K Anomaly in  $\text{LaFeAsO}$ : Competing Antiferromagnetic Interactions, Frustration, and a Structural Phase Transition, *Phys. Rev. Lett.* **101**, 057010 (2008).
- [82] J. Glasbrenner, I. Mazin, H. O. Jeschke, P. Hirschfeld, R. Fernandes, and R. Valentí, Effect of magnetic frustration on nematicity and superconductivity in iron chalcogenides, *Nature Physics* **11**, 953 (2015).
- [83] M. Hirayama, T. Misawa, T. Miyake, and M. Imada, Ab initio studies of magnetism in the iron chalcogenides fete and fese, *Journal of the Physical Society of Japan* **84**, 093703 (2015).
- [84] E. Abrahams and Q. Si, Quantum criticality in the iron pnictides and chalcogenides, *Journal of Physics: Condensed Matter* **23**, 223201 (2011).
- [85] I. M. Hayes, R. D. McDonald, N. P. Breznay, T. Helm, P. J. Moll, M. Wartenbe, A. Shekhter, and J. G. Analytis, Scaling between magnetic field and temperature in the high-temperature superconductor  $\text{BaFe}_2(\text{As}_{1-x}\text{P}_x)_2$ , *Nature Physics* **12**, 916 (2016).
- [86] D. Chowdhury, B. Swingle, E. Berg, and S. Sachdev, Singularity of the London Penetration Depth at Quantum Critical Points in Superconductors, *Phys. Rev. Lett.* **111**, 157004 (2013).
- [87] A. Levchenko, M. G. Vavilov, M. Khodas, and A. V. Chubukov, Enhancement of the London Penetration Depth in Pnictides at the Onset of Spin-Density-Wave Order under Superconducting Dome, *Phys. Rev. Lett.* **110**, 177003 (2013).
- [88] S. Kasahara, T. Shibauchi, K. Hashimoto, K. Ikada, S. Tonegawa, R. Okazaki, H. Shishido, H. Ikeda, H. Takeya, K. Hirata, T. Terashima, and Y. Matsuda, Evolution from non-Fermi- to Fermi-liquid transport via isovalent doping in  $\text{BaFe}_2(\text{As}_{1-x}\text{P}_x)_2$  superconductors, *Phys. Rev. B* **81**, 184519 (2010).
- [89] X. Lu, J. Park, R. Zhang, H. Luo, A. H. Nevidomskyy, Q. Si, and P. Dai, Nematic spin correlations in the tetragonal state of uniaxial-strained  $\text{BaFe}_{2-x}\text{Ni}_x\text{As}_2$ , *Science* **345**, 657 (2014).
- [90] J.-H. Chu, J. G. Analytis, K. De Greve, P. L. McMahon, Z. Islam, Y. Yamamoto, and I. R. Fisher, In-Plane Resistivity Anisotropy in an Underdoped Iron Arsenide Superconductor, *Science* **329**, 824 (2010).
- [91] M. A. Tanatar, E. C. Blomberg, A. Kreyssig, M. G. Kim, N. Ni, A. Thaler, S. L. Bud'ko, P. C. Canfield, A. I. Goldman, I. I. Mazin, and R. Prozorov, Uniaxial-strain mechanical detwinning of  $\text{CaFe}_2\text{As}_2$  and  $\text{BaFe}_2\text{As}_2$  crystals: Optical and transport study, *Phys. Rev. B* **81**, 184508 (2010).
- [92] C. Mirri, A. Dusza, S. Bastelberger, M. Chinotti, L. Degiorgi, J.-H. Chu, H.-H. Kuo, and I. R. Fisher, Origin of the Resistive Anisotropy in the Electronic Nematic Phase of  $\text{BaFe}_2\text{As}_2$  Revealed by Optical Spectroscopy, *Phys. Rev. Lett.* **115**, 107001 (2015).
- [93] T.-M. Chuang, M. P. Allan, J. Lee, Y. Xie, N. Ni, S. L. Bud'ko, G. S. Boebinger, P. C. Canfield, and J. C. Davis, Nematic Electronic Structure in the "Parent" State of the Iron-Based Superconductor  $\text{Ca}(\text{Fe}_{1-x}\text{Co}_x)_2\text{As}_2$ , *Science* **327**, 181 (2010).
- [94] E. P. Rosenthal, E. F. Andrade, C. J. Arguello, R. M. Fernandes, L. Y. Xing, X. Wang, C. Jin, A. J. Millis, and A. N. Pasupathy, Visualization of electron nematicity and unidirectional antiferroic fluctuations at high temperatures in  $\text{NaFeAs}$ , *Nature Physics* **10**, 225 (2014).
- [95] S. Liang, A. Moreo, and E. Dagotto, Nematic State of Pnictides Stabilized by Interplay between Spin, Orbital, and Lattice Degrees of Freedom, *Phys. Rev. Lett.* **111**, 047004 (2013).
- [96] L. Fanfarillo, A. Cortijo, and B. Valenzuela, Spin-orbital interplay and topology in the nematic phase of iron pnictides, *Phys. Rev. B* **91**, 214515 (2015).
- [97] C.-C. Lee, W.-G. Yin, and W. Ku, Ferro-Orbital Order and Strong Magnetic Anisotropy in the Parent Compounds of Iron-Pnictide Superconductors, *Phys. Rev. Lett.* **103**, 267001 (2009).
- [98] W. Lv, F. Krüger, and P. Phillips, Orbital ordering and unfrustrated  $(\pi, 0)$  magnetism from degenerate double exchange in the iron pnictides, *Phys. Rev. B* **82**, 045125 (2010).
- [99] Y. Yamakawa, S. Onari, and H. Kontani, Nematicity and Magnetism in FeSe and Other Families of Fe-Based Superconductors, *Phys. Rev. X* **6**, 021032 (2016).
- [100] C. Fang, H. Yao, W.-F. Tsai, J. Hu, and S. A. Kivelson, The-

- ory of electron nematic order in LaFeAsO, *Phys. Rev. B* **77**, 224509 (2008).
- [101] C. Xu, M. Müller, and S. Sachdev, Ising and spin orders in the iron-based superconductors, *Phys. Rev. B* **78**, 020501 (2008).
- [102] R. M. Fernandes, P. P. Orth, and J. Schmalian, Intertwined Vestigial Order in Quantum Materials: Nematicity and Beyond, *Annual Review of Condensed Matter Physics* **10**, 133 (2019).
- [103] F. Wang, S. A. Kivelson, and D.-H. Lee, Nematicity and quantum paramagnetism in fese, *Nature Physics* **11**, 959 (2015).
- [104] R. M. Fernandes, A. V. Chubukov, J. Knolle, I. Eremin, and J. Schmalian, Preemptive nematic order, pseudogap, and orbital order in the iron pnictides, *Phys. Rev. B* **85**, 024534 (2012).
- [105] E. Gati, L. Xiang, S. L. Bud'ko, and P. C. Canfield, Role of the Fermi surface for the pressure-tuned nematic transition in the BaFe<sub>2</sub>As<sub>2</sub> family, *Phys. Rev. B* **100**, 064512 (2019).
- [106] R. M. Fernandes, A. E. Böhmer, C. Meingast, and J. Schmalian, Scaling between Magnetic and Lattice Fluctuations in Iron Pnictide Superconductors, *Phys. Rev. Lett.* **111**, 137001 (2013).
- [107] S. Baek, D. Efremov, J. Ok, J. Kim, J. van den Brink, and B. Büchner, Orbital-driven nematicity in FeSe, *Nature Materials* **14**, 210 (2015).
- [108] A. E. Böhmer, K. Kothapalli, W. T. Jayasekara, J. M. Wilde, B. Li, A. Sapkota, B. G. Ueland, P. Das, Y. Xiao, W. Bi, J. Zhao, E. E. Alp, S. L. Bud'ko, P. C. Canfield, A. I. Goldman, and A. Kreyssig, Distinct pressure evolution of coupled nematic and magnetic orders in FeSe, *Phys. Rev. B* **100**, 064515 (2019).
- [109] P. Zhang, T. Qian, P. Richard, X. P. Wang, H. Miao, B. Q. Lv, B. B. Fu, T. Wolf, C. Meingast, X. X. Wu, Z. Q. Wang, J. P. Hu, and H. Ding, Observation of two distinct  $d_{xz}/d_{yz}$  band splittings in FeSe, *Phys. Rev. B* **91**, 214503 (2015).
- [110] H. Pfau, S. D. Chen, M. Yi, M. Hashimoto, C. R. Rotundu, J. C. Palmstrom, T. Chen, P.-C. Dai, J. Straquadine, A. Hristov, R. J. Birgeneau, I. R. Fisher, D. Lu, and Z.-X. Shen, Momentum Dependence of the Nematic Order Parameter in Iron-Based Superconductors, *Phys. Rev. Lett.* **123**, 066402 (2019).
- [111] S. Lederer, Y. Schattner, E. Berg, and S. A. Kivelson, Superconductivity and non-Fermi liquid behavior near a nematic quantum critical point, *Proceedings of the National Academy of Sciences* **114**, 4905 (2017).
- [112] A. Klein and A. V. Chubukov, Superconductivity near a nematic quantum critical point: Interplay between hot and lukewarm regions, *Phys. Rev. B* **98**, 220501 (2018).
- [113] T. Worasaran, M. S. Ikeda, J. C. Palmstrom, J. A. Straquadine, S. A. Kivelson, and I. R. Fisher, Nematic quantum criticality in an Fe-based superconductor revealed by strain-tuning, arXiv:2003.12202 (2020).
- [114] T. Shibauchi, T. Hanaguri, and Y. Matsuda, Exotic Superconducting States in FeSe-based Materials, *Journal of the Physical Society of Japan* **89**, 102002 (2020).
- [115] A. I. Coldea, Electronic nematic states tuned by isoelectronic substitution in bulk FeSe<sub>1-x</sub>S<sub>x</sub>, arXiv:2009.05523 (2020).
- [116] K. Okazaki, Y. Ota, Y. Kotani, W. Malaeb, Y. Ishida, T. Shimojima, T. Kiss, S. Watanabe, C.-T. Chen, K. Kihou, C. H. Lee, A. Iyo, H. Eisaki, T. Saito, H. Fukazawa, Y. Kohori, K. Hashimoto, T. Shibauchi, Y. Matsuda, H. Ikeda, H. Miyahara, R. Arita, A. Chainani, and S. Shin, Octet-Line Node Structure of Superconducting Order Parameter in KFe<sub>2</sub>As<sub>2</sub>, *Science* **337**, 1314 (2012).
- [117] P. J. Hirschfeld, Using gap symmetry and structure to reveal the pairing mechanism in fe-based superconductors, *Comptes Rendus Physique* **17**, 197 (2016).
- [118] T.-H. Lee, A. V. Chubukov, H. Miao, and G. Kotliar, Pairing Mechanism in Hund's Metal Superconductors and the Universality of the Superconducting Gap to Critical Temperature Ratio, *Phys. Rev. Lett.* **121**, 187003 (2018).
- [119] V. Stanev and Z. Tešanović, Three-band superconductivity and the order parameter that breaks time-reversal symmetry, *Phys. Rev. B* **81**, 134522 (2010).
- [120] V. Grinenko, R. Sarkar, K. Kihou, C. Lee, I. Morozov, S. Aswartham, B. Büchner, P. Chekhonin, W. Skrotzki, K. Nenkov, R. Hühne, K. Nielsch, S. L. Drechsler, V. L. Vadimov, M. A. Silaev, P. A. Volkov, I. Eremin, H. Luetkens, and H. H. Klauss, Superconductivity with broken time-reversal symmetry inside a superconducting s-wave state, *Nature Physics* **16**, 789 (2020).
- [121] U. Karahasanovic and J. Schmalian, Elastic coupling and spin-driven nematicity in iron-based superconductors, *Phys. Rev. B* **93**, 064520 (2016).
- [122] I. Paul and M. Garst, Lattice Effects on Nematic Quantum Criticality in Metals, *Phys. Rev. Lett.* **118**, 227601 (2017).
- [123] P. Reiss, D. Graf, A. A. Haghghirad, W. Knafo, L. Drigo, M. Bristow, A. J. Schofield, and A. I. Coldea, Quenched nematic criticality and two superconducting domes in an iron-based superconductor, *Nature Physics* **16**, 89 (2020).
- [124] A. P. Dioguardi, M. M. Lawson, B. T. Bush, J. Crocker, K. R. Shirer, D. M. Nisson, T. Kissikov, S. Ran, S. L. Bud'ko, P. C. Canfield, S. Yuan, P. L. Kuhns, A. P. Reyes, H.-J. Grafe, and N. J. Curro, NMR evidence for inhomogeneous glassy behavior driven by nematic fluctuations in iron arsenide superconductors, *Phys. Rev. B* **92**, 165116 (2015).
- [125] B. A. Frandsen, Q. Wang, S. Wu, J. Zhao, and R. J. Birgeneau, Quantitative characterization of short-range orthorhombic fluctuations in FeSe through pair distribution function analysis, *Phys. Rev. B* **100**, 020504 (2019).
- [126] R. J. Koch, T. Konstantinova, M. Abeykoon, A. Wang, C. Petrovic, Y. Zhu, E. S. Bozin, and S. J. L. Billinge, Room temperature local nematicity in FeSe superconductor, *Phys. Rev. B* **100**, 020501 (2019).
- [127] H.-H. Kuo, J.-H. Chu, J. C. Palmstrom, S. A. Kivelson, and I. R. Fisher, Ubiquitous signatures of nematic quantum criticality in optimally doped Fe-based superconductors, *Science* **352**, 958 (2016).
- [128] D. Huang and J. E. Hoffman, Monolayer FeSe on SrTiO<sub>3</sub>, *Annual Review of Condensed Matter Physics* **8**, 311 (2017).
- [129] H. Hosono, A. Yamamoto, H. Hiramatsu, and Y. Ma, Recent advances in iron-based superconductors toward applications, *Materials Today* **21**, 278 (2018).
- [130] L. Boeri, O. V. Dolgov, and A. A. Golubov, Is LaFeAsO<sub>1-x</sub>F<sub>x</sub> an Electron-Phonon Superconductor?, *Phys. Rev. Lett.* **101**, 026403 (2008).
- [131] S. Mandal, R. E. Cohen, and K. Haule, Strong pressure-dependent electron-phonon coupling in FeSe, *Phys. Rev. B* **89**, 220502 (2014).
- [132] J. Lee, F. Schmitt, R. Moore, S. Johnston, Y.-T. Cui, W. Li, M. Yi, Z. Liu, M. Hashimoto, Y. Zhang, *et al.*, Interfacial mode coupling as the origin of the enhancement of  $T_c$  in FeSe films on SrTiO<sub>3</sub>, *Nature* **515**, 245 (2014).
- [133] C. Platt, W. Hanke, and R. Thomale, Functional renormalization group for multi-orbital fermi surface instabilities, *Advances in Physics* **62**, 453 (2013).
- [134] H. Kontani and S. Onari, Orbital-Fluctuation-Mediated Superconductivity in Iron Pnictides: Analysis of the Five-Orbital Hubbard-Holstein Model, *Phys. Rev. Lett.* **104**, 157001 (2010).

- [135] C.-T. Chen, C. Tsuei, M. Ketchen, Z.-A. Ren, and Z. Zhao, Integer and half-integer flux-quantum transitions in a niobium-iron pnictide loop, *Nature Physics* **6**, 260 (2010).
- [136] K. Cho, M. Kończykowski, S. Teknowijoyo, M. A. Tanatar, and R. Prozorov, Using electron irradiation to probe iron-based superconductors, *Superconductor Science and Technology* **31**, 064002 (2018).
- [137] H. Yang, Z. Wang, D. Fang, Q. Deng, Q.-H. Wang, Y.-Y. Xiang, Y. Yang, and H.-H. Wen, In-gap quasiparticle excitations induced by non-magnetic Cu impurities in  $\text{Na}(\text{Fe}_{0.96}\text{Co}_{0.03}\text{Cu}_{0.01})\text{As}$  revealed by scanning tunnelling spectroscopy, *Nature Communications* **4**, 2749 (2013).
- [138] K. Kuroki, H. Usui, S. Onari, R. Arita, and H. Aoki, Pnictogen height as a possible switch between high- $T_c$  nodeless and low- $T_c$  nodal pairings in the iron-based superconductors, *Phys. Rev. B* **79**, 224511 (2009).
- [139] O. Vafek and A. V. Chubukov, Hund Interaction, Spin-Orbit Coupling, and the Mechanism of Superconductivity in Strongly Hole-Doped Iron Pnictides, *Phys. Rev. Lett.* **118**, 087003 (2017).
- [140] W.-C. Lee, S.-C. Zhang, and C. Wu, Pairing State with a Time-Reversal Symmetry Breaking in FeAs-Based Superconductors, *Phys. Rev. Lett.* **102**, 217002 (2009).
- [141] F. Kretzschmar, B. Muschler, T. Böhm, A. Baum, R. Hackl, H.-H. Wen, V. Tsurkan, J. Deisenhofer, and A. Loidl, Raman-Scattering Detection of Nearly Degenerate  $s$ -Wave and  $d$ -Wave Pairing Channels in Iron-Based  $\text{Ba}_{0.6}\text{K}_{0.4}\text{Fe}_2\text{As}_2$  and  $\text{Rb}_{0.8}\text{Fe}_{1.6}\text{Se}_2$  Superconductors, *Phys. Rev. Lett.* **110**, 187002 (2013).
- [142] V. K. Thorsmølle, M. Khodas, Z. P. Yin, C. Zhang, S. V. Carr, P. Dai, and G. Blumberg, Critical quadrupole fluctuations and collective modes in iron pnictide superconductors, *Phys. Rev. B* **93**, 054515 (2016).
- [143] Y. Gallais, I. Paul, L. Chauvière, and J. Schmalian, Nematic Resonance in the Raman Response of Iron-Based Superconductors, *Phys. Rev. Lett.* **116**, 017001 (2016).
- [144] F. Tafti, A. Juneau-Fecteau, M.-E. Delage, S. R. De Cotret, J.-P. Reid, A. Wang, X. Luo, X. Chen, N. Doiron-Leyraud, and L. Taillefer, Sudden reversal in the pressure dependence of  $T_c$  in the iron-based superconductor  $\text{KFe}_2\text{As}_2$ , *Nature Physics* **9**, 349 (2013).
- [145] S. Rinott, K. B. Chashka, A. Ribak, E. D. L. Rienks, A. Taleb-Ibrahimi, P. Le Fevre, F. Bertran, M. Randeria, and A. Kanigel, Tuning across the BCS-BEC crossover in the multiband superconductor  $\text{Fe}_{1+y}\text{Se}_x\text{Te}_{1-x}$ : An angle-resolved photoemission study, *Science Advances* **3**, e1602372 (2017).
- [146] L. Kong, S. Zhu, M. Papaj, H. Chen, L. Cao, H. Isobe, Y. Xing, W. Liu, D. Wang, P. Fan, *et al.*, Half-integer level shift of vortex bound states in an iron-based superconductor, *Nature Physics* **15**, 1181 (2019).
- [147] X. Wu, R.-X. Zhang, G. Xu, J. Hu, and C.-X. Liu, In the Pursuit of Majorana Modes in Iron-based High- $T_c$  Superconductors, arXiv:2005.03603 (2020).
- [148] L.-Y. Kong and H. Ding, Emergent vortex Majorana zero mode in iron-based superconductors, *Acta Physica Sinica* **69**, 110301 (2020).
- [149] H. Lohani, T. Hazra, A. Ribak, Y. Nitzav, H. Fu, B. Yan, M. Randeria, and A. Kanigel, Band inversion and topology of the bulk electronic structure in  $\text{FeSe}_{0.45}\text{Te}_{0.55}$ , *Phys. Rev. B* **101**, 245146 (2020).
- [150] P. Zhang, Z. Wang, X. Wu, K. Yaji, Y. Ishida, Y. Kohama, G. Dai, Y. Sun, C. Bareille, K. Kuroda, *et al.*, Multiple topological states in iron-based superconductors, *Nature Physics* **15**, 41 (2019).
- [151] M. Chen, X. Chen, H. Yang, Z. Du, X. Zhu, E. Wang, and H.-H. Wen, Discrete energy levels of Caroli-de Gennes-Matricorn states in quantum limit in  $\text{FeTe}_{0.55}\text{Se}_{0.45}$ , *Nature communications* **9**, 970 (2018).
- [152] D. Wang, L. Kong, P. Fan, H. Chen, S. Zhu, W. Liu, L. Cao, Y. Sun, S. Du, J. Schneeloch, R. Zhong, G. Gu, L. Fu, H. Ding, and H.-J. Gao, Evidence for Majorana bound states in an iron-based superconductor, *Science* **362**, 333 (2018).
- [153] T. Machida, Y. Sun, S. Pyon, S. Takeda, Y. Kohsaka, T. Hanaguri, T. Sasagawa, and T. Tamegai, Zero-energy vortex bound state in the superconducting topological surface state of  $\text{Fe}(\text{Se},\text{Te})$ , *Nature Materials* **18**, 811 (2019).
- [154] J.-X. Yin, Z. Wu, J. Wang, Z. Ye, J. Gong, X. Hou, L. Shan, A. Li, X. Liang, X. Wu, *et al.*, Observation of a robust zero-energy bound state in iron-based superconductor  $\text{Fe}(\text{Te},\text{Se})$ , *Nature Physics* **11**, 543 (2015).
- [155] C. Chen, K. Jiang, Y. Zhang, C. Liu, Y. Liu, Z. Wang, and J. Wang, Atomic line defects and zero-energy end states in monolayer  $\text{Fe}(\text{Te},\text{Se})$  high-temperature superconductors, *Nature Physics* **16**, 536 (2020).
- [156] Z. Wang, J. O. Rodriguez, L. Jiao, S. Howard, M. Graham, G. D. Gu, T. L. Hughes, D. K. Morr, and V. Madhavan, Evidence for dispersing 1D Majorana channels in an iron-based superconductor, *Science* **367**, 104 (2020).
- [157] Y. Li, N. Zaki, V. O. Garlea, A. T. Savici, D. Fobes, Z. Xu, F. Camino, C. Petrovic, G. Gu, P. D. Johnson, J. M. Tranquada, and I. A. Zaliznyak, Magnetic, superconducting, and topological surface states on  $\text{Fe}_{1+y}\text{Te}_{1-x}\text{Se}_x$ , arXiv:2012.07893 (2020).
- [158] E. J. König and P. Coleman, Crystalline-Symmetry-Protected Helical Majorana Modes in the Iron Pnictides, *Phys. Rev. Lett.* **122**, 207001 (2019).
- [159] R.-X. Zhang, W. S. Cole, and S. Das Sarma, Helical Hinge Majorana Modes in Iron-Based Superconductors, *Phys. Rev. Lett.* **122**, 187001 (2019).
- [160] N. Heinsdorf, M. H. Christensen, M. Iraola, S. Zhang, F. Yang, T. Birol, C. D. Batista, R. Valentí, and R. M. Fernandes, Prediction of Double-Weyl Points in the Iron-Based Superconductor  $\text{CaKFe}_4\text{As}_4$ , arXiv:2101.05301 (2021).
- [161] L. Kong, L. Cao, S. Zhu, M. Papaj, G. Dai, G. Li, P. Fan, W. Liu, F. Yang, X. Wang, *et al.*, Tunable vortex Majorana zero modes in  $\text{LiFeAs}$  superconductor, arXiv:2010.04735 (2020).
- [162] N. Katayama, K. Kudo, S. Onari, T. Mizukami, K. Sugawara, Y. Sugiyama, Y. Kitahama, K. Iba, K. Fujimura, N. Nishimoto, M. Nohara, and H. Sawa, Superconductivity in  $\text{Ca}_{1-x}\text{La}_x\text{FeAs}_2$ : A Novel 112-Type Iron Pnictide with Arsenic Zigzag Bonds, *Journal of the Physical Society of Japan* **82**, 123702 (2013).
- [163] E. Dagotto, Colloquium: The unexpected properties of alkali metal iron selenide superconductors, *Rev. Mod. Phys.* **85**, 849 (2013).
- [164] S. Wu, B. A. Frandsen, M. Wang, M. Yi, and R. Birgeneau, Iron-Based Chalcogenide Spin Ladder  $\text{BaFe}_2\text{X}_3$  ( $X = \text{Se}, \text{S}$ ), *Journal of Superconductivity and Novel Magnetism* **33**, 143 (2020).
- [165] A. V. Maharaj, E. W. Rosenberg, A. T. Hristov, E. Berg, R. M. Fernandes, I. R. Fisher, and S. A. Kivelson, Transverse fields to tune an Ising-nematic quantum phase transition, *Proceedings of the National Academy of Sciences* **114**, 13430 (2017).